2.1. CONDENSED MATTER PHYSICS

CONTENTS

Polarized Neutrons

Study of Depth Profiles of Elements of Thin Layer Structures Using RBS Technique
A.P.Kobzev, D.A.Korneev, O.A.Nikonov, V.A.Ul'yanov, B.G.Peskov, N.K.Pleshanov, V.M.Pusenkov, E.V.Siber Z.N.Soroko, V.G.Syromyatnikov, A.F.Schebetov

Off-Specular Neutron Reflection from Magnetic Media with Nondiagonal Reflectivity Matrices
D.A.Korneev, V.I.Bodnarchuk, V.K.Ignatovich

Investigation of the Hg-1201 structure under high external pressure by means of neutron diffraction.

V.L.Aksenov, A.M.Balagurov, B.N.Savenko, D.V.Sheptyakov
Dubna, JINR, Frank Lab of Neutron Physics, Russia
V.P.Glazkov, V.A.Somenkov
Russian Scientific Center "Kurchatov Institute", Moscow, Russia
E.V.Antipov, S.N.Putilin
Moscow State University, Department of Chemistry, Russia

$HgBa_2CuO_{4+\delta}$ is the first member of the homologous series of mercury-based superconductors[1] with general composition $HgBa_2Ca_{n-1}Cu_nO_{2n+2+\delta}$. This family of superconducting compounds displays the highest values of T_c available by now. Moreover their superconducting transition temperatures raise with the increase of external pressure[2,3] with practically the same speed for all the representatives of the series, approximately 2 K/GPa. For example it has been reported that the T_c's of above 150 K had been achieved for the compound with n=3 (Hg-1223) at external pressures higher than 10 GPa.

The increase of T_c induced by external pressure is being observed to some extent in all hole-doped superconducting copper oxides. This shows that the basic physical reason for this phenomenon is the same for all of them. It is naturally to suppose that this reason is the change in free charges concentration in the superconducting layers CuO_2 caused by changes in the interatomic distances.

Diffraction methods are providing the direct information concerning structural changes in crystals, and neutron diffraction seems to be the best method for investigations of the High-T_c compounds because it is necessary to determine the positions of the oxygen atoms with high precision. But it is quite complicated problem to obtain the information on the charge transfer even with the use of neutron diffraction because the changes of the interatomic distances are very small and the accuracy of the experimental data turns out to be insufficient. One of the ways to solve this problem is the increase of the accuracy of the data obtained, which is of course possible if the experiments are carried out at the diffractometer with the resolution (in the interlayer distances scale) not worse than 0.003. Though it is usually possible to carry out such an experiment in the range of pressures up to 1 GPa, the accuracy of the evaluated interatomic distances is quite satisfactory to make qualitative conclusions. Another possibility is in significant increase of the range of pressures at the sample (3-5 GPa) which allows to obtain necessary accuracy of data on the diffractometers with the resolution on the level of 0.01.

The structural changes in mercury-based superconductors caused by applying high external pressure have already been the subject of investigations for several teams of explorers[5,6]. In [5] the authors have investigated the crystal structures of $HgBa_2CuO_{4+\delta}$ and $HgBa_2CaCu_2O_{6+\delta}$ with a pressure up to 0.6 GPa and $HgBa_2Ca_2Cu_3O_{8+\delta}$ with a pressure up to 9.2 GPa by means of neutron powder diffraction. They have obtained the values of the compressibilities along the *a*- and *c*-axes and the bond distances compressibilities as well. In[6] the team of investigators have studied the pressure-induced structural changes in $HgBa_2Ca_1Cu_2O_{6+\delta}$ by means of neutron powder diffraction at the DN-12 diffractometer in Dubna in the pressure range 0-3.6 GPa with the use of sapphire anvil high-pressure cell. The lattice constants and bond distances compressibilities were determined and analyzed

involving quite doubtful model of disordered in the plane (*a,b*) oxygen but nevertheless the results turned out to be in general good agreement with the other data: the distance between Ba and O2 had the highest compressibility among all the other bond distances, and the compressibility of the *c*-axis is approximately twice higher than of the *a*-axis.

The structure of the compound with n=1 (Hg-1201) is the simplest among all the other compounds of the mercury series and other high-T_c's, and this is an important prerequisite for investigation of the small changes in the structure. Another important circumstance is that this compound is usually being obtained practically without any impurities and the analysis is not distorted by the signs of the other phases. As the compound with n=1 (Hg-1201) has the most simple structure among all the others, the aim of this investigation was to determine the general character of the structural behavior of Hg-1201 under applied high external pressure.

The experiments were carried out at the DN-12[4] specialized diffractometer for microsamples investigations at the IBR-2 pulsed reactor in Dubna. We used the sapphire-anvils high pressure cell to create the desirable pressures at the sample. At each pressure we have managed to perform the neutron diffraction experiment at two different angles simultaneously (usually these scattering angles values were near 45° and 90°). Such simultaneous measurements have ensured us in the correct and comparatively precise determination of experimental conditions and, thus, of the values of interest. The pressure was measured by detecting the displacement of the ruby luminescence lines and the uncertainty of these determinations was 0.03 GPa. The experiments were carried out at zero pressure in the region of d_{hkl} from 1.0 to 5.0 Å on the pure sample of the volume approximately 20 mm^3 in order to clarify the original structure and at pressures 1.47, 3.14, 4.31 and 5.07 GPa in the region of d_{hkl} from 1.8 to 5.0 Å in the high pressure cell (sample volume ≤ 2 mm^3). Rietveld refinement procedures of the diffraction patterns obtained at zero pressure possessed to estimate the values of the coordinates of atoms in the original structure. The quality of the diffraction patterns at intermediate pressures 1.47 and 3.14 GPa was not sufficient for precise determination of the lattice geometry because of the high level of background and the presence of parasitic diffraction from the sapphire single-crystal anvils but it turned out to be good enough to obtain the values of the lattice constants. Due to special improvements of the sample environment (background suppression, first of all) the quality of the diffraction patterns at higher pressures of 4.31 and 5.07 GPa turned out to be significantly better and this allowed us to carry out Rietveld refinement procedures with variation of several structural parameters, namely the *z*-coordinates of Ba and apical O atoms and lattice parameters as well. The typical view of the parts of the Rietveld refinements of the $HgBa_2CuO_{4+\delta}$ structure at zero pressure and at high pressure are shown in the fig. 1 and the detailed results of the diffraction patterns treatments are presented in the table 1.

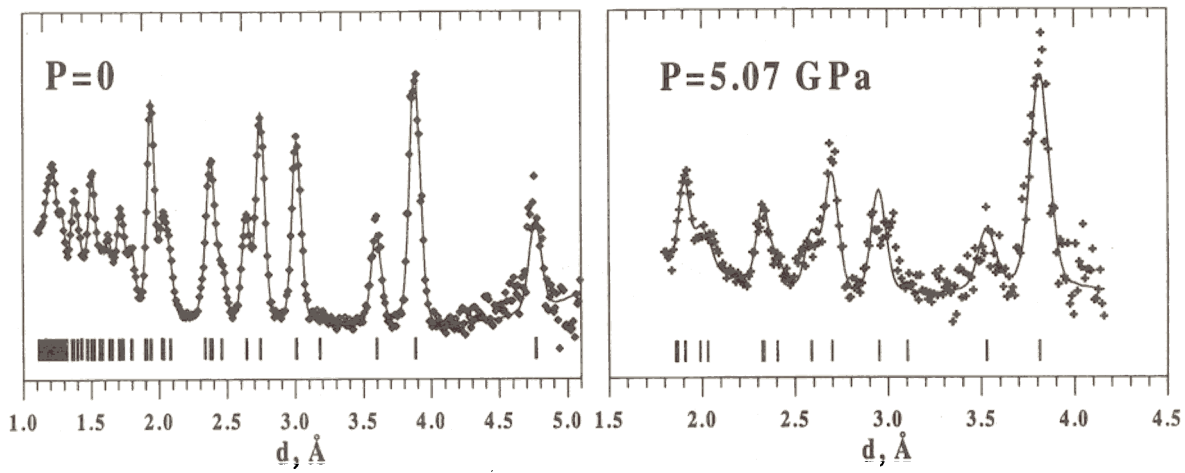

fig. 1. The parts of the Rietveld refinements of $HgBa_2CuO_{4+\delta}$ structure.

Table 1. Results of the Rietveld refinements of the $HgBa_2CuO_{4+\delta}$ structure under high external pressure.

Param.\ P(GPa)	0	1.47	3.14	4.31	5.07
a, Å	3.882(1)	3.852(2)	3.835(2)	3.826(2)	3.815(2)
c, Å	9.527(2)	9.462(8)	9.358(7)	9.335(8)	9.308(7)
V, $Å^3$	143.6	140.4	137.6	136.6	135.5
Hg, n	0.95	0.95	0.95	0.95	0.95
B, $Å^2$	1.5(3)			0.8(6)	1
Ba, z	0.2981(4)			0.299(2)	0.296(2)
B, $Å^2$	0.6			0.6	0.6
Cu, n	1	1	1	1	1
B, $Å^2$	0.5	0.5	0.5	0.5	0.5
O1, n	2	2	2	2	2
B, $Å^2$	1	1	1	1	1
O2, z	0.2078(4)			0.212(2)	0.212(2)
B, $Å^2$	1			1	1
O3, n	0.12			0.12	0.12
B, $Å^2$	1			1	1
R_w, %	4	8.5	9.2	8.8	8.8
χ^2	1.8	1.3	2.2	1.7	2.5
Cu-O2, Å	2.784			2.688	2.681
Hg-O2, Å	1.980			1.979	1.973
Ba/*l*-Cu/*l*, Å	1.924			1.876	1.899
Ba/*l*-O2/*l*, Å	0.860			0.812	0.782
Ba/*l*-Hg/*l*, Å	2.840			2.791	2.755

The main result of these experiments were the dependencies of the lattice parameters versus pressure (see fig. 2) and the dependencies of some interatomic distances in $HgBa_2CuO_{4+\delta}$ versus pressure (fig. 3, fig. 4); so we've really obtained the values of the compressibilities of the $HgBa_2CuO_{4+\delta}$ structure along *a* and *c* axes, the volume compressibility of the unit cell, and approximately estimated the compressibilities of some selected bond distances in the structure (see table 2).

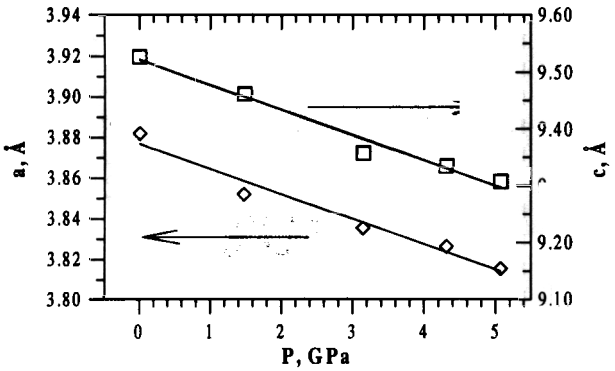

fig. 2. Lattice constants of $HgBa_2CuO_{4+\delta}$ structure versus pressure.

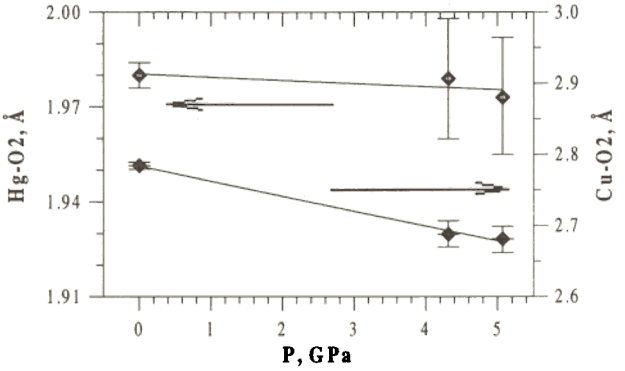

fig. 3. Dependencies of some interatomic distances in $HgBa_2CuO_{4+\delta}$ structure versus pressure.

Table 2. Compressibilities of the lattice parameters and of the unit cell volume of the $HgBa_2CuO_{4+\delta}$ structure as determined from the neutron powder diffraction data ($k_q=-(1/q)\delta q/\delta P$ (10^{-3} GPa^{-1})).

k_a	3.4
k_c	4.5
k_V	11.1
$k_{Ba/l\text{-}O2/l}$	18
$k_{Cu\text{-}O2}$	7.3
$k_{Hg\text{-}O2}$	0.7

The values of the lattice constants compressibilities are in general good agreement with those obtained earlier for the other members of the series[5,6]. The presence of small anisotropy in the lattice constants compressibilities is also in good agreement with earlier results[5,6]. Our measurements have shown that the pressure-induced changes in the $HgBa_2CuO_{4+\delta}$ structure really occur: the apical oxygen to copper atom distance sharply shortens with pressure increase (corresponding compressibility is $7.3*(10^{-3}$ $GPa^{-1})$) while the interatomic distance between O2 and Hg atoms remains practically the same.

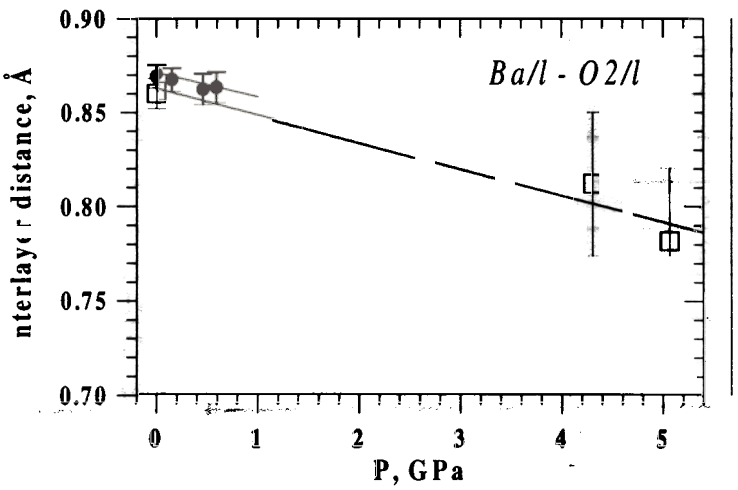

fig. 4. Dependence of Ba-O2 splitting in $HgBa_2CuO_{4+\delta}$ structure versus pressure. (● - data from[5], - current investigation)

It has been shown in the earlier works[7,8] that the value of interlayer splitting between Ba and O2 layers is the most sensitive value to the charge state of the basic and CuO_2 planes. Moreover, reasonable suggestions on the charge transfer between these two planes can be done on the basis of this splitting value. We present the dependence of this interlayer splitting on pressure in the fig. 4 together with the data

obtained in[5]. It is quite obvious that the two sets of data are giving practically the same behavior of the Ba-O2 splitting with pressure. This value is the most compressible parameter in the structure (as well as in the other members of the Hg-based compounds): $k_{Ba\text{-}O2} \approx 18$. It can be calculated that the corresponding value from[5] is approximately $k_{Ba\text{-}O2} \approx 15$.

From the charge balance analysis it follows that the decrease of Ba-O2 splitting corresponds to the charge transfer from the HgO_δ reservoir to the CuO_2 plane. In order to estimate this charge transfer it is possible[8] to use the empiric equation $\Delta = -0.045 + 0.2475Q$ which puts up the correlation between the splitting of the Ba-O2 layers and the charge transfer between the neighbouring HgO_δ and CuO_2 planes. Using this equation and our results we obtained that at external pressure of 5.07 GPa the charge equal to 0.13 elementary charges travels to the CuO_2 planes. This value after being normalized to the 1 GPa pressure is close to those obtained in[8] for Y-123, Y-124 and Hg-1212. This flow of charge from basic layers to the superconducting ones causes the lowering of the formal charge of copper atoms which results in the increase of the onset temperature. These speculations explain qualitatively the growth of T_c with pressure the observations of which had been reported about elsewhere[2,3].

Acknowledgements

We thank V.A.Alyoshin and D.A.Mikhailova for sample preparation.

References

1. E.V.Antipov, S.N.Putilin, Priroda (in Russia), 10 (1994) 3
2. C.W. Chu, L.Gao, F.Chen, Z.I.Huang, R.L.Meng and Y.Y.Xue, Nature, (London), 365 (1993) 323
3. M.Nunez-Regueiro, J.Tholence, E.V.Antipov, J.Capponi and M.Marezio, Science 262 (1993) 97
4. V.L.Aksenov et al, High Press. Res. 14 (1995) 181
5. B.A.Hunter, J.D.Jorgensen, J.L.Wagner, P.G.Radaelli et al, Physica C 221 (1994) 1
6. V.L.Aksenov et al, High Press. Res. 14 (1995) 127
7. S.Sh.Shilshtein, A.S.Ivanov, V.A.Somenkov, Physica C, 245 (1995) 181
8. S.Sh.Shilshtein, IAE Communications, 5339/9, Moscow, 1995

PHASE TRANSITION IN AC_{60} (A=K,Rb) FULLERIDE CRYSTALS

V.L. Aksenov, Yu.A. Ossipyan*, V.S. Shakhmatov

Frank Laboratory of Neutron Physics, JINR, Dubna
*ISSP, RAS, Chernogolovka, Russia

From experimental investigations, e.g., [1], it is known that the phase transition (PT) from the high temperature face-centered cubic phase of the Fm3m (O_h^5) symmetry to the low temperature polymeric-like phase of the Pnnm (D_{2h}^{12}) orthorhombic symmetry is observed in AC_{60} (A=K,Rb) fulleride crystals.

Inter-arrangement of the crystal cells of the above two phases is shown in Fig. 1.

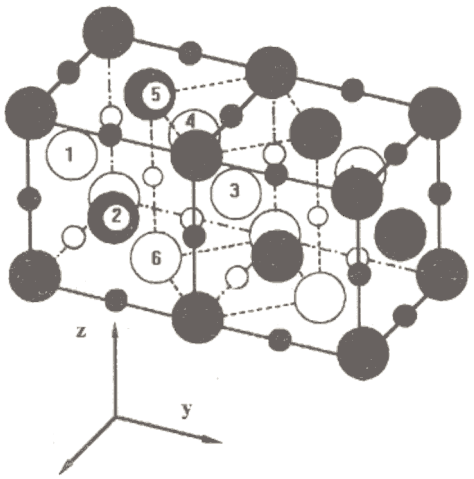

Fig. 1. Inter-arrangement of crystal cells in the Fm3m and Pnnm phases. Large circles refer to C_{60} molecules, smaller circles refer to metal atoms. Black circles indicate metal atoms and C_{60} molecules situated on visible faces of two face-centered cubic cells in the Fm3m phase. The Pnnm phase crystal cell is shown by dashed lines. The C_{60} molecules creating the octahedral environment for the metal atom are denoted by the numbers 1,...,6.

The A C_{60} compounds exhibit a number of very interesting physical properties. In the Fm3m high temperature phase, these compounds demonstrate strong localization of electrons, while in the polymeric-like phase, the A C_{60} compounds are quasi-one-dimensional metals. Moreover, at low temperatures the metallic state is unstable with respect to the formation of spin or charge density waves [2].

In our paper [3], the Landau phenomenological theory of PT to a polymeric-like phase in A C_{60} (A=K,Rb) crystals is developed on the basis of symmetry analysis. By analysis of the interactions between order parameters, probable PT connected

changes in the subsystem of metal atoms are investigated. The developed theory predicts the partial ordering of alkali metal atoms over the positions allowed in the octahedral environment of C_{60} molecules (Fig. 2).

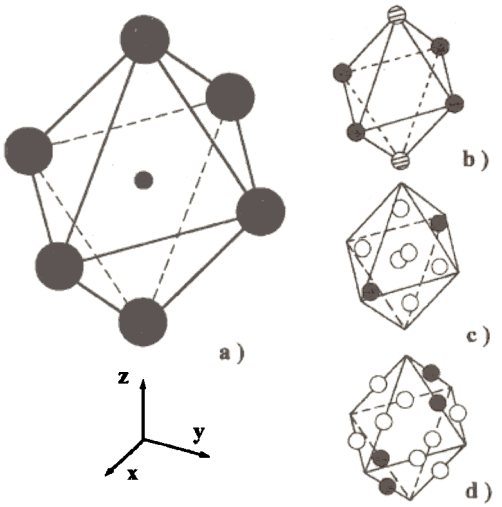

Fig.2. Possible types of positions for metal atoms (smaller circles) in the octahedral environment of C_{60} molecules (large circles): a) The central position **1b**; b), c) and d) are the **6e**, **8f** and **12i** positions, respectively.

A metal atom in the octahedral **1b** center position (Fig.2a) experiences no structural changes following PT. If a metal atom occupies a noncentral position, then partial ordering over the positions indicated in Figs. 2b, c), and d) takes place following PT. For the **6e** position, the partial ordering of the metal atoms either on the horizontal plane (dark circles) or over two positions situated above or below the plane (shaded circles) takes place. For the **8f** and **12i** positions (Fig. 2c and d), the occupied positions are shown by dark circles.

At decreasing temperature the appearance of another structural PT, which leads to complete ordering of the metal atoms, is also possible.

References

1. P.W. Stephens, G. Bortel, G. Faigel et al., *Nature*, **370**, 636 (1994).

2. O. Chauvet, G. Oszlanyi, L. Forro et al., *Phys. Rev. Lett.*,**72**, 2721 (1994).

3. V.L. Aksenov, Yu.A. Ossipyan, V.S. Shakhmatov, *JETP Letters*, **62**, 428 (1995) and
Preprint JINR, E17-95-426, Dubna, 1995.

Precision neutron diffraction structural study of the high-T_c superconductor $HgBa_2CuO_{4+\delta}$

A.M.Balagurov, V.V.Sikolenko, V.G.Simkin
141980 Dubna, JINR, Frank Lab of Neutron Physics, Russia

V.A.Aleshin, E.V.Antipov, D.A.Michajlova, S.N.Putilin
119899 Moscow State University, Department of Chemistry, Russia

F.Bouree
91191 Gif-sur-Yvette, LLB, France

The new mercury superconductors, belonging to a series of the general formula $HgBa_2Ca_{n-1}Cu_nO_{2+2n+\delta}$, with n=1,2,3 etc., were discovered in 1993[1]. The highest transition temperature, 134 K, was found for n=3. It increases up to 150 K under pressure of 11 GPa and this value is a record for high-T_c materials at present.

The structure of Hg-based compounds is being investigated by all possible methods, neutron diffraction among them. Several questions are still open, first of all about the exact oxygen content and its connection with T_c, about the mercury occupancy factor, and the reason for the high mercury temperature factor.

At FLNP, the studies of these new compounds were initiated in 1994 and continued in 1995. These studies are carried out in collaboration with the MSU Department of Chemistry of and the Russian Scientific Center of Kurchatov Institute. In 1995, four $HgBa_2CuO_{4+\delta}$ (Hg-1201) samples were studied: sample A with $T_c \approx 71$ K, m=2.09 g, sample B with $T_c \approx 83$ K, m=2.05 g, sample C with $T_c \approx 98$ K, m=1.93 g and sample D with $T_c \approx 96$ K, m=1.84 g. The last was prepared by a special method that resulted in an unconventional relation between the *a* and *c* lattice parameters. The main goal of this study was determination of the T_c dependence on oxygen content.

Neutron diffraction experiments with those samples were performed on the high resolution Fourier diffractometer (HRFD) at the IBR-2 pulsed reactor in Dubna and the 3T2 diffractometer at the Orphee reactor in Saclay. Diffraction pattern measurements were done with HRFD at room temperature for samples A-D and at 8 K for sample B. With 3T2, the measurements were made of sample A at room temperature and at 8 K. All the observed diffraction lines were accounted for by the expected Hg-1201 structure with the symmetry of space group *P4/mmm*. The MRIA and FULLPROF programs were used for processing data. A refinement of the Fourier spectra was carried out in the 0.81 - 2.09 Å interval with 110 peaks from Hg-1201. An example of the measured diffraction pattern can be seen in Fig.1. The refinement was done for the *z*-coordinates of Ba and O2 atoms, for the occupancy factors of Hg and O3 atoms, and for temperature factors of all atoms except O3. The determined structural data, together with selected interatomic and interlayer distances, are given in Table 1. The small amount of O3 atoms in the structure did not allow the exact value of the temperature factor, B_T(O3), to be found, though the correlation with the O3 occupancy factor, n(O3), was not very high. Thus, the variation of B_T(O3) over wide limits did not change n(O3) more than the limit of one standard deviation. A much stronger correlation was found between B_T(Hg) and n(Hg) (Fig.2). Moreover, for these two parameters, the minimum in χ^2 and R-factors values is not very pronounced.

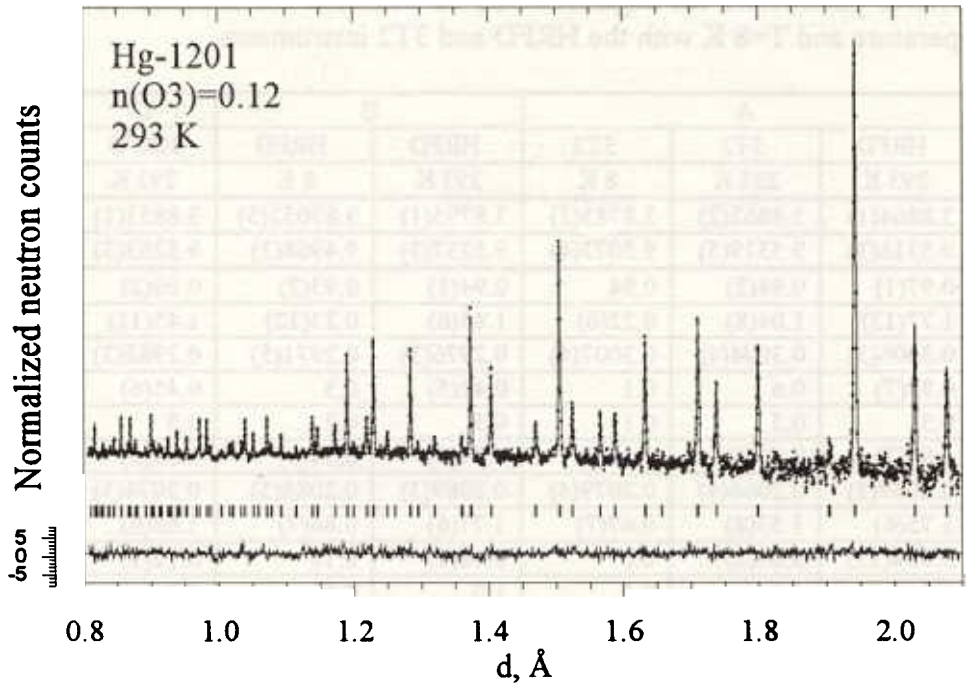

Fig. Diffraction spectrum from $HgBa_2CuO_{4.12}$, measured with the HRFD diffractometer and processed by the Rietveld method.

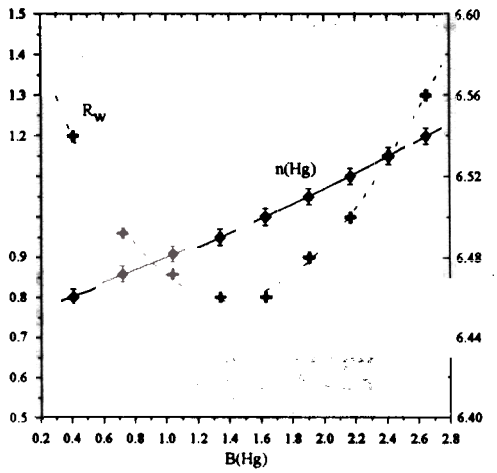

Fig. 2 Mercury occupancy factor n(Hg) (left scale) and weighted R_w-factor (right scale) as functions of a fixed value of B_T(Hg) for sample C.

On the whole, the structural results are in good accordance with published data[2-4] and, especially, with the data of Ref.[5] All features of the Hg-1201 structure and their dependence on temperature and oxygen content announced in[4] were confirmed.

We would like to draw special attention to the deficiency of the Hg position and the large temperature factors of the Hg and O2 atoms. The first was already mentioned in papers[6] and[7]. The attempts to explain it as a substitution of mercury for impurity atoms (copper or carbon) lead to contradictions with other data[6]. The low temperature data show that B_T(Hg) and B_T(O2) become much smaller at T=8 K. So, we have come to the conclusion that the mercury deficiency is real and the temperature motion of the Hg and O3 atoms is actually high at room temperature.

Both for our samples and the samples studied in[5], the linear dependence between oxygen content and the values of the *a* and *c* parameters can be seen. The T_c value depends strongly on n(O3), as shown in Figure 3, where our data and data from[5] are displayed. As it was predicted, both curves are hill-like, though their maximums are shifted.

Table 1. Structural parameters for $HgBa_2CuO_{4+\delta}$ as obtained for samples A - D at room temperature and T=8 K with the HRFD and 3T2 instruments.

Sample	A			B		C	D
Instrument	HRFD	3T2	3T2	HRFD	HRFD	HRFD	HRFD
Param./ T, K	293 K	293 K	8 K	293 K	8 K	293 K	293 K
a, Å	3.8864(1)	3.8862(2)	3.8783(2)	3.8795(1)	3.87052(5)	3.8851(1)	3.8851(1)
c, Å	9.5316(3)	9.5319(5)	9.5073(4)	9.5237(3)	9.4968(3)	9.5263(3)	9.5202(3)
Hg, n	0.97(1)	0.94(2)	0.94	0.94(1)	0.93(2)	0.96(2)	0.91(2)
B, $Å^2$	1.77(12)	1.04(8)	0.22(6)	1.45(6)	0.23(12)	1.45(11)	1.09(15)
Ba, z	0.3006(3)	0.3004(4)	0.3007(4)	0.2976(3)	0.2971(5)	0.2982(3)	0.2981(3)
B, $Å^2$	0.89(7)	0.6	0.1	0.42(5)	0.3	0.45(6)	0.29(7)
Cu, B, $Å^2$	0.5	0.5	0.1	0.5	0.2	0.5	0.5
O1, B, $Å^2$	1.06(7)	0.70(8)	0.38(8)	0.77(5)	0.34(8)	0.64(6)	0.29(7)
O2, z	0.2059(3)	0.2066(4)	0.2079(4)	0.2089(3)	0.2088(5)	0.2074(3)	0.2082(3)
B, $Å^2$	1.75(6)	1.53(8)	0.67(7)	1.77(6)	0.86(7)	1.68(6)	1.58(7)
O3, n	0.054(11)	0.07(2)	0.07	0.18(1)	0.18	0.12(1)	0.11(1)
B, $Å^2$	1.0	1.0	0.5	1.0	0.5	1.0	1.0
R_w	0.068			0.059	0.056	0.065	0.077
χ^2	1.06	1.18	1.21	1.78	1.06	1.07	1.11
Cu-O2, Å	2.803(3)	2.797(4)	2.777(4)	2.772(3)	2.765(5)	2.787(3)	2.778(3)
Hg-O2, Å	1.963(3)	1.969(4)	1.977(4)	1.990(3)	1.983(5)	1.975(3)	1.982(3)
Hg-Cu, Å	4.766	4.766	4.754	4.762	4.748	4.762	4.760
Ba// - Cu//, Å	1.901(3)	1.903(4)	1.895(4)	1.928(3)	1.927(5)	1.922(3)	1.922(3)
Ba// - O2//, Å	0.903(4)	0.894(5)	0.882(5)	0.845(4)	0.839(7)	0.865(4)	0.856(4)
Ba// - Hg//, Å	2.865(3)	2.863(4)	2.859(4)	2.834(3)	2.821(5)	2.834(3)	2.838

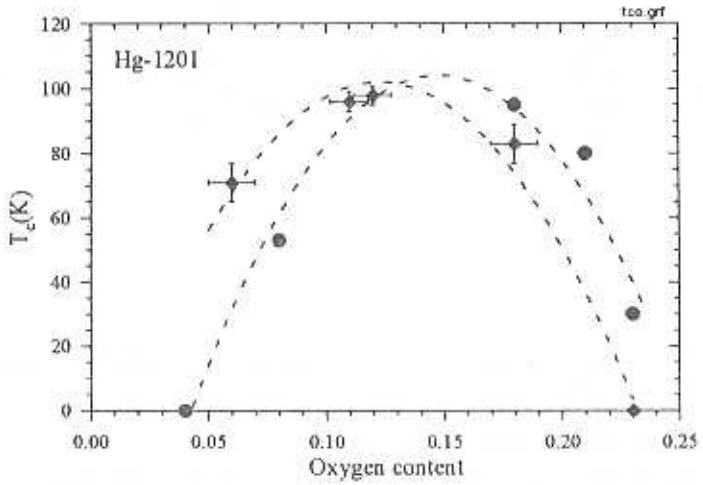

Fig. 3 T_c as a function of oxygen content for our samples (◊) together with point (δ=0.23) from[4] and for samples from paper[5] (•). The dashed curves are eye guides.

For the studied interval of oxygen content, the most pronounced changes can be found in the interlayer Ba - O2 distance, namely ~0.06 Å. It is ~10 times larger than the change in the *c* lattice parameter. This fact is in accordance with the idea published in[8] that this distance is the most sensitive one to charge changes in the neighboring layers. But the experimental decrease in this distance with increasing of δ does not coincide to the calculated value if the valence of the O3 atoms is put at −2. The coincidence can be achieved following the suggestion that ν(O3)≈−0.98. This value is in good accordance with the formal valence calculations performed in[5], where for ν(O3) the value of −0.90 was found.

In structural Hg-1201 papers, the question about the exact cation content of the compound is under very active discussion. Direct refinement attempts using the Rietveld

method failed due to the small number of additional atoms and the influence of experimental error. More information can be obtained after calculating the scattering-density maps, especially of experimental and calculated difference densities. The very high resolution of HRFD offers the possibility of drawing these maps. The sensitivity of this method is illustrated in Fig.4, where the difference map for the basal plane sample A is shown. The O3 atom is seen very clearly; its peak amplitude is ~2.5 times higher than the highest background peaks. It means that atoms with a coherent scattering length of ~0.6 (carbon, for instance) can be found for a concentration of around 3%. As an example, the experimental scattering-density map for the x=y, $0 \leq z \leq 0.5$ section is shown in Fig.5.

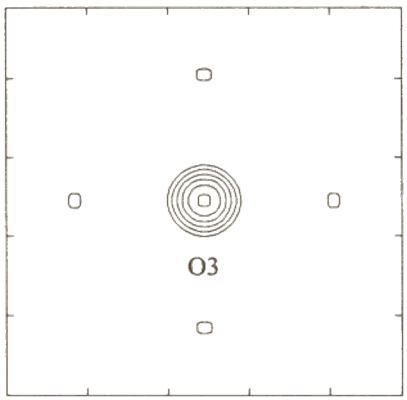

Fig. 4 Difference scattering-density map for the basal plane of sample. Oxygen O3 was removed from the for calculation of F_{hkl}.

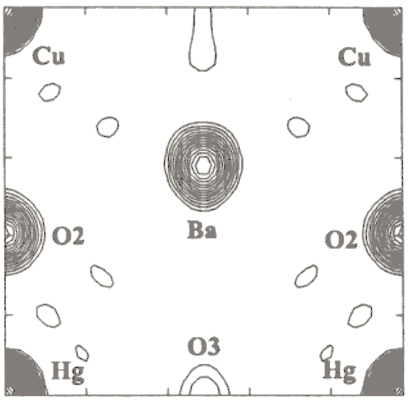

Fig. 5 Experimental scattering-density map for the diagonal crosssection x=y, $0 \leq z \leq 0.5$ of sample C.

References

1 S.N.Putilin, E.V.Antipov, O.Chmaissem and M.Marezio, Nature (London), 362 (1993) 226.
2. J.L.Wagner et al., *Physica C*, 210 (1993) 447.
3. O.Chmaissem et al., *Physica C*, 212 (1993) 259.
4. S.M.Loureiro et al., *Physica C*, 243 (1993) 1.
5. Q.Huang, J.W.Lynn, Q.Xiong, C.W.Chu, *Phys. Rev.*, B52 (1995) 462.
6. E.T Alexandre, S.M.Loureiro, E.V.Antipov et al., *Physica C*, 245 (1995) 207.
7. V.L.Aksenov, E.V.Antipov, A.M.Balagurov et al., *High Press. Res.*, 14 (1995) 127.
8. S.Sh.Shilstein, A.S.Ivanov, V.A.Somenkov, *Physica C*, 245 (1995) 181.

Structure of Graphitized Carbon Black Aggregates in Triton X-100/Water Solutions by Small Angle Neutron Scattering.

Vasil M. Garamus, Frank Laboratory of Neutron Physics Joint Institute for Nuclear Research, Dubna, Russsia; Jan Skov Pedersen Risø National Laboratory, Roskilde, Denmark; Leonid L. Bulavin, Kiev University, Kiev, Ukraine; Tamara V. Karmazina Institute of Colloid Chemistry and Chemistry of Water, Kiev, Ukraine.

Small angle neutron scattering method gives unique information about inner structure of carbon black (CB) particles [1]. The measurements of CB/Triton X-100/water solutions were continue of the such kind experiments at Risø National Laboratory performed by us [2]. The main conclusions of Ref. [2] are that the presence of CB particles shift CMC of Triton X-100 and fractal like CB particles with adsorbed layer of Triton X-100 and Triton X-100 micelles are situated at solutions.

In present measurements the experimental beam time was 18 h at half reactor power (1 MW) that is why only two experiments were performed in two different contrasts 30% and 60% heavy water.

The views of all curves agree with obtained previously [2]. In 30% heavy water solution we can observe only CB particles and in case 60% CB particles with adsorbed layer of Triton X-100 and Triton X-100 micelles give contributions to scattering curves.

The lower part of curves (q=0.008-0.02 $Å^{-1}$) were analysed by simple fractal expression:

$$d\Sigma(q)/d\Omega \sim q^{-D},$$

where D is the fractal dimension. The obtained values of D are 3.44±0.06 and 2.74±0.04 for 30% and 60% respectively together with early obtained [2] point that the compensation point is situated between 75 and 100% heavy water content.

The experimental scattering curves obtained in this experiment and previously [2] were modelled by expression:

$$d\Sigma(q)/d\Omega = A_1\Delta^2\rho_{CB}\Phi^2(q,<R>,\sigma,L)S(q,D,\zeta) + A_2\Delta^2\rho_{TP}F^2_{el}(q,a,\nu) + A_3\rho^2_sF^2_{sph}(q,r) + A_4,$$

where first term describe the scattering from fractals consist of polydisperse primary spherical particles with average radius <R> and dispersion σ, L - width of Triton layer, ζ is the maximum size of fractal structure; the second term is the scattering of ellipsoid of rotation Triton X-100 micelles with little semiaxis a and ratio between axis ν; the third term is a scattering from spherical voids which present in CB particles; A_4 is residual background.

The experimental data and model curves are represented at figure which shows good agreement between it.

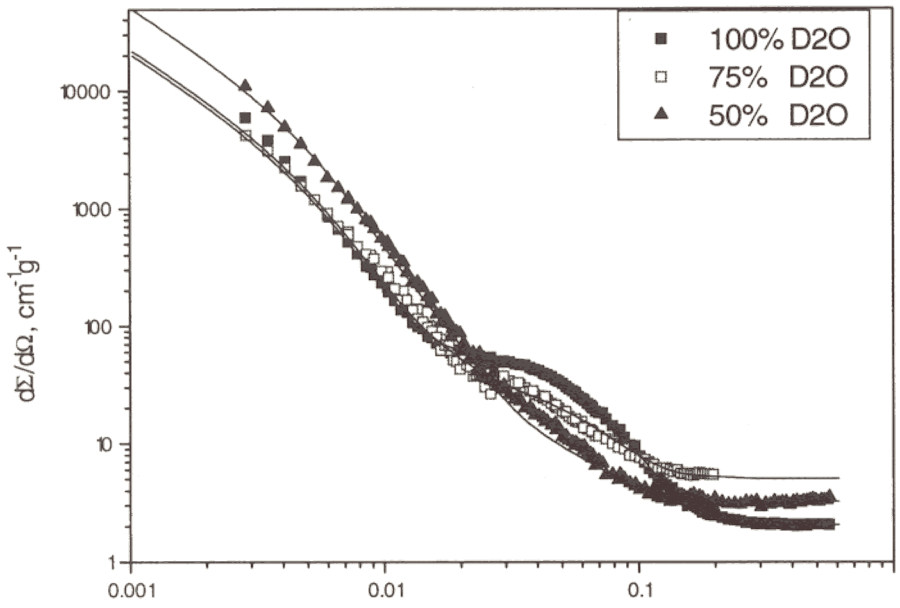

Small angle neutron scattering by dispersion of 10 g/l CB in 1.84 g/l Triton X-100/water solution with different contrast and model (solid lines).

The fractal dimension is found to decrease for increasing CB concentration from D = 3.4 at h = 0.01 to D = 2.9 at h = 0.05, the maximum size of fractal aggregate increases from 150 Å to 200 Å. The primary CB particles have wide size distribution and it's average size (80 Å) slightly decreases with CB concentration. The degree of occupation of CB surface by surfactant molecules is 10% and stays the constant with varying CB and surfactant concentration. The micelle structure is found same to it's structure in surfactant/water solutions. The volume fraction of voids does not exceed 1% of CB volume fraction.

1. Hjelm R. P. Jr., Wampler W. A., Seeger P. A. / J. Mater. Res., 1994, v. 9, p. 3210-3222.
2. Garamus V.M., Pedersen J.S. 2.7.6 "Carbon Black Dispersion in Non-Ionic Surfactant Water Solutions" "Annual Progress Reports of Department of Solid State Physics 1 January - 31 December 1994" ed. P.-A. Lindgard, K. Bechgaard, K. N. Clausen, R. Feidenhans'l, and I. Johannsen, Riso National Laboratory, Roskilde, Denmark, 1995 p.98

Structure of mixed multilayers of palmitoyloleoylphosphatidylcholine and oligooxyethelene glycol monododecyl ether determined by x-ray and neutron diffraction.

G. Klose[1], A. Islamov[2], B. Koenig[1] and V. Cherezov[2].

(1) University of Leipzig, Germany.

(2) LNP JINR Dubna, Russia.

Structure analysis of the lipid multilayers modified by nonionic surfactant was carried out at DN-2 diffractometer for studying several fundamental questions concerning structural and dynamical properties of lipid/water interfaces, understanding intermembrane interactions and the nature of so-called hydration forces.The structure of palmitoyl-oleoylphosphatidylcholine lipid (POPC) containing nonionic surfactant of the type $C_{12}H_{25}O(CH_2CH_2O)_nH$ ($C_{12}E_n$) was studied at the relative humidities RH=85%, 97% and at the molar ratio surfactant/lipid $R_{A/L}$=0.5,1, with n=2,4 and 6, where n is number of hydrophilic oxyethelene moieties. Partially deuterated surfactants $C_{12}H_{25}O(\mathbf{CD_2CD_2O})_nH$ ($C_{12}E_n$-d4n) and $C_{11}H_{23}\mathbf{CD_2}O(CH_2CH_2O)_nH$ ($C_{12}E_n$-d2) were used to determine the location of surfactants in lipid matrix. Fig.1. presents strip-function models of deuterated segments together with electron density profiles of POPC/$C_{12}E_n$ bilayers determined by x-ray diffraction. It was shown that α-methylene position ($C_{12}E_n$-d2 label) is anchored near the boundary of the hydrophobic core of lipid matrix, the oxyethelene moieties($C_{12}E_n$-d4n label) are mainly located in the polar membrane/water interface. With increasing humidity , molar ratio surfactant/lipid and number of oxyethelene moieties n, the partial lose of areas under strip-models is observed. This can be explained by the high degree of static disorder or/and motional freedom of surfactant moieties in the lipid matrix.

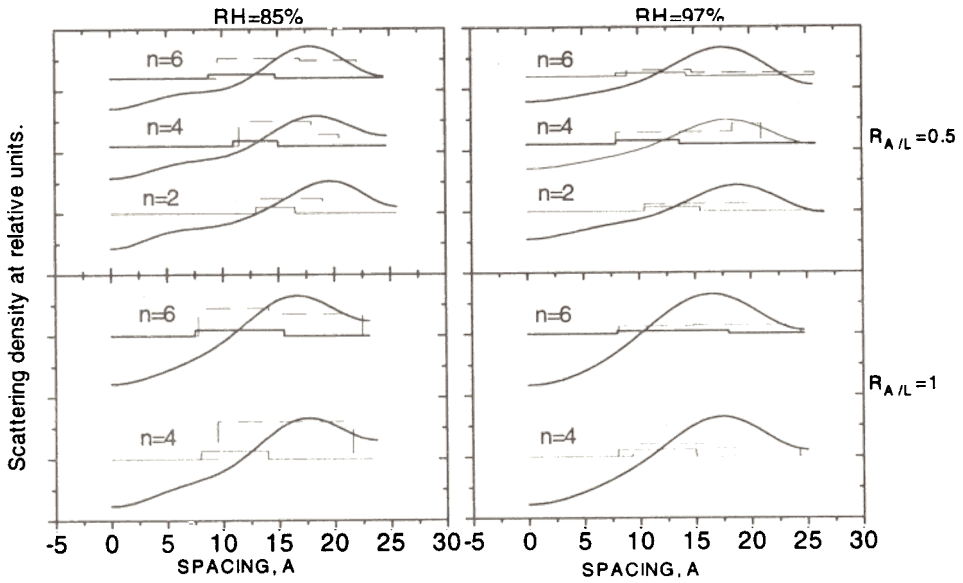

Fig.1. Strip-function models of deuterated segments $C_{12}E_n$-d2(solid line) and $C_{12}E_n$-d4n (dashed line) are presented together with electron density profiles of POPC/$C_{12}E_n$ bilayers at the relative humidities RH=85% and 97%, molar ratio surfactant/lipid $R_{A/L}$=0.5 and 1, n=2,4 and 6. Dramatical decrease of the area under deuterated label evidences about high degree of disorder of oxyethelene moieties in the lipid bilayer.

Partially unfolded state of lysozymes in dimethylsulphoxide with a well developed secondary structure

M.V.Avdeev*, M.D.Kirkitadze**, D.A.Prokhorov**, I.N.Serdyuk*, A.A.Timchenko**

* Frank Laboratory of Neutron Physics, Joint Institute for Nuclear Research, Dubna
** Institute of Protein Research, Puschino

A structural description of intermediate states realized upon spontaneous protein folding is ultimately essential for an understanding of protein self-organization rules. In most cases, however, kinetic intermediates have life times too short to be fully studied. It is more fruitful to find experimental conditions where the intermediates are stable. An example are low-molecular alcohols that stabilize the protein intermediate called a 'molten globule'. The action of dimethylsulfoxide (DMSO) on protein structure is the most interesting. It was shown for hen-egg white lysozyme (HEWL) that the helicity of unfolded protein in DMSO becomes somewhat higher than the helicity of the native one, and the protein forms a gel at low pH. These facts are indicative of great changes in the protein conformation and strong intermolecular interactions. Up to now, no structural information about these states has been available.

To fill this gap, we used neutron scattering from a solution of HEWL in DMSO and light water. The use of X-ray scattering for these purposes is practically impossible because of the high absorbance of X-rays by DMSO. The scattering experiments of HEWL in 70% DMSO at pH 2.5 and pH 2.0 have been performed. The latter case corresponds to the case of gel formation. The range of scattering vectors was 0.008 - 0.25 $Å^{-1}$. Figure 1 presents the scattering curve of HEWL in 70% DMSO at pH 2.5 plotted on Kratky coordinates. Such a plot makes it possible to distinguish the globular structure from the unfolded one. The wide plateau on this plot represents a coil-like structure. On the contrary, the globular structure shows a complex picture in this region, as can be seen from Fig.2 for the globular chaperonin GroEL measured simultaneously with HEWL.

Analysis of the plot in Fig.1 shows a plateau with a small incline. It indicates that the coil-like structure of the lysozyme molecule differs from the ideal coil. From the Guinier plot in the small-angle region, it is possible to evaluate the radius of gyration and intensity at the zero scattering angle I(0). Knowing I(0) it is easy to calculate the molecular mass of the protein. Such calculations have been made and it appears that lysozyme in 70% DMSO consists of about two monomers and its radius of gyration Rg is 35 Å. Such an Rg value unambiguously means that the conformation of the protein is not compact, in contrast to the 'molten globule' state. It is possible that the conformation of HEWL in DMSO resembles an early stage of protein folding where, according to some

investigators, unfolded conformation with native-like helices is formed. Further model calculations can clarify this question.

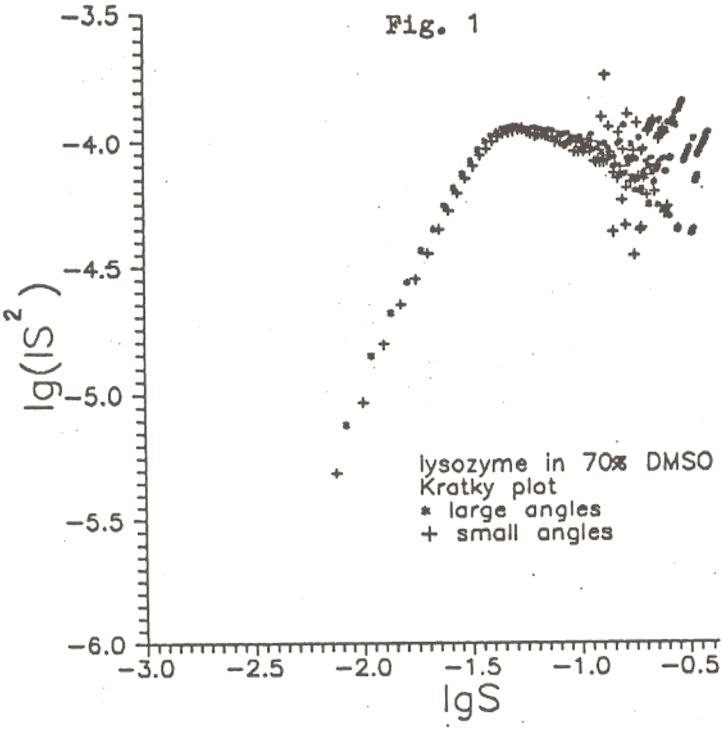

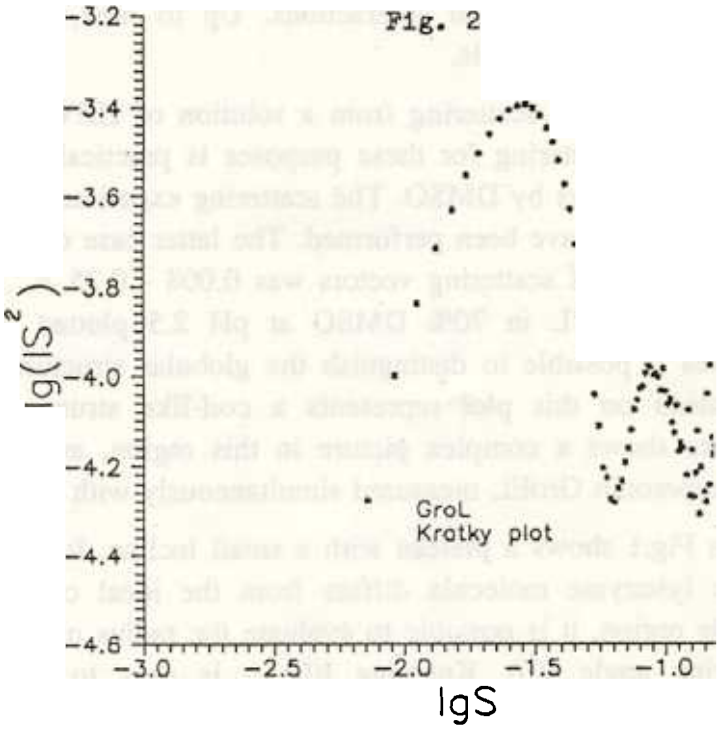

Some problems appeared upon measuring the gel-like form of the protein, but they can be easily solved after some changes in the program of data treatment. The above results will be published in the journal of Biofizika.

References

[1] K.Braig, Z.Otwinowski, R.Hegde, D.C.Boisvert, A.Joachimiak, A.L.Horwich, P.B.Sigler Nature, 371, 578-585 (1994)

[2] L.M.Gierasch, Z.Wang, J.Hunt, S.J.Landry, A.Weaver, J.Deisenhofer, Prot. Engineering 8 suppl.,14 (1995)

[3] K.Braig, M.Simon, F.Furuya, J.F.Hainfeld, A.L.Horwich, Proc. Natl. Acad. Sci. USA, 90, 3978-3982 (1993)

[4] Y.Igarashi, K.Kimura, K.Ichimura, S.Matsuzaki, T.Ikura, K.Kuwajima, H.Kihara, Biochemistry (1995, in press)

[5] D.I.Svergun J.Appl.Cryst. 24, 485-492 (1991)

Ammonium dynamics in $K_{1-x}(NH_4)_xI$ mixed salts at 10 K.

I. Natkaniec[&], L.S. Smirnov, S.I. Bragin, A.I. Solov'ev

Frank Laboratory of Neutron Physics, JINR, 141980 Dubna, Russia
&-On leave from H. Niewodniczanski Institute of Nuclear Physics, 31-342 Krakow, Poland

The $K_{1-x}(NH_4)_xI$ mixed salts have attracted increasing interest because they exhibit a low-temperature orientational glass phase devoid of long range order. The orientational degrees of freedom involved in the disordered frozen state are related to induced electric dipoles associated with the ammonium tetrahedra [1]. The x-T phase diagram of the $K_{1-x}(NH_4)_xI$ solid solution has been determined in [2] as consisting of three concentration ranges at low temperatures. At high concentrations ($x > x_c \cong 0.75$), ammonium ions are ordered as in pure NH_4I in a slightly distorted CsCl structure of tetragonal symmetry. For $0.3<x<x_c$ an orientational glassy phase with short range antiferroelectric order manifests itself in a NaCl type cubic structure. At cooling, below $x \cong 0.3$, the transition is no longer collective but is replaced by a single ion freezing.

The low energy rotational tunnelling transitions ($\Delta E < 1$ meV) have been investigated by the inelastic incoherent neutron scattering (IINS) method for $x<0.30$, but the rotational tunnelling states of ammonium ions in a diluted solutions of $K_{1-x}(NH_4)_xI$ are still not well understood [3,4]. The IINS studies of the localised dynamics in the dipolar $K_{1-x}(NH_4)_xI$ glass within the range $0.05<x<0.70$ show three distinct ammonium excitations at ca. 10, 21 and 31 meV, which are interpreted in terms of the so-called "triple-approach model" assuming that the tetrahedral ammonium ions adopt the C_{3v} symmetry site in the crystal [5].

We have studied the $K_{1-x}(NH_4)_xI$ system in the full concentration range on the NERA spectrometer at the IBR-2 pulsed reactor [6]. The IINS spectra were measured for concentrations x=0.0, 0.05, 0.15, 0.30, 0.45, 0.60, 0.80 and 1.0 at temperatures of 10, 80 and 290 K, respectively. The G(E) weighted phonon density of states obtained from the IINS spectra at 10 K are presented in Fig. 1.

The G(E) of pure potassium iodide exhibits two bands with energies of 5.8 and 13.2 meV, which correspond to the acoustic and optic phonon branches, respectively, in accordance with ref. [7]. For ammonium concentrations below x_c, corresponding G(E) functions display an additional low energy excitation at ca. 2.5 meV, in comparison to the results of ref. [5]. The low energy bands at ca. 2.5 and 9 meV are present only in the G(E) of the disordered phase. In the ordered, phase translational and torsional ammonium vibrations are marked by ν_5 and ν_6, respectively. The ν_5 band broadening with increasing ammonium concentration and in the ordered phase demonstrates two maxima. The average energy of the translational ammonium vibrations slightly decreases with ammonium concentration. The energy of the torsional excitations ν_6 changes from 36.5 meV in the ordered phase to ca. 30 meV in the disordered phase. The width of these bands increases with decreasing ammonium concentration.

The concentration dependencies of the energies of the ammonium excitations in the $K_{1-x}(NH_4)_xI$ mixed salts at 10 K are presented in Fig. 2 and are compared with the results of ref. [5].

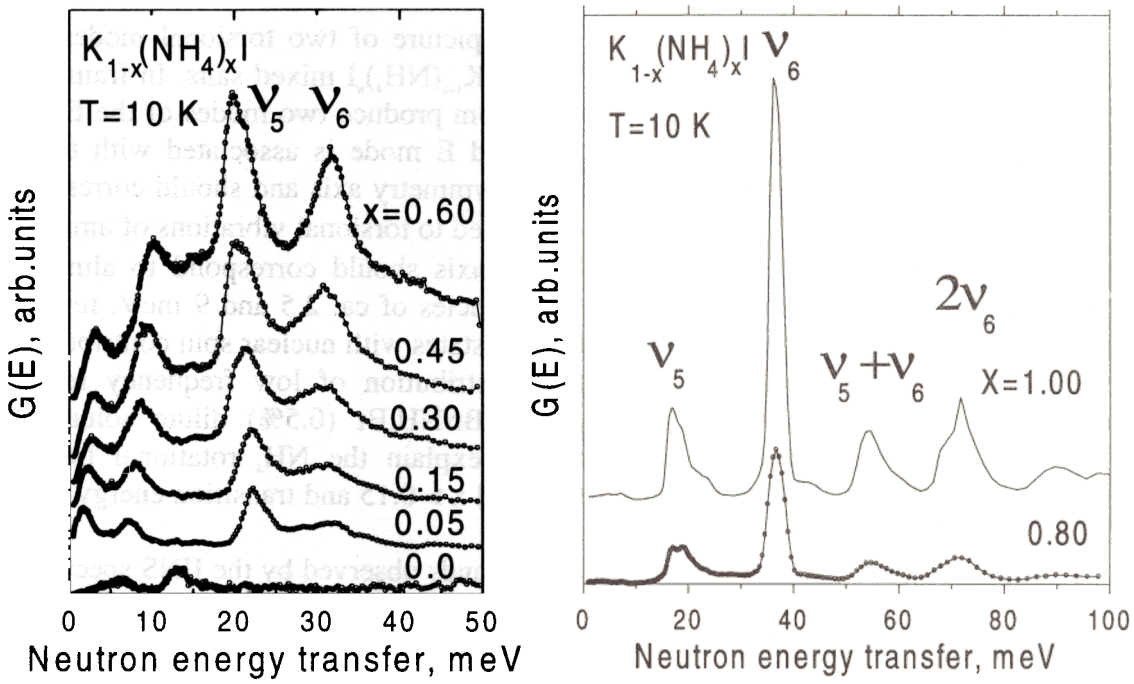

Fig. 1. The concentration dependence of the G(E) spectra for the $K_{1-x}(NH_4)_xI$ samples at 10 K.

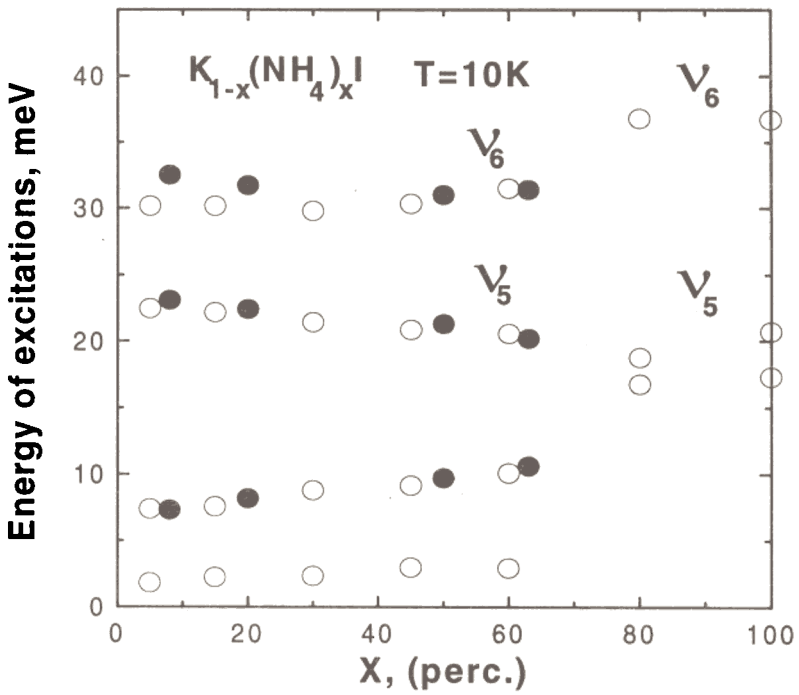

Fig. 2. The concentration dependence of the excitation energies of ammonium ions in $K_{1-x}(NH_4)_xI$ mixed salts (O- our results, O- results of ref. [5]).

Our results do not confirm the simple picture of two torsional modes of the ammonium ions in the disordered phase of the $K_{1-x}(NH_4)_xI$ mixed salts. In frame of the C_{3v} model, the three rotational degrees of freedom produce two modes of the E and A_2 character, respectively. The doubly degenerated E mode is associated with torsional vibrations about axes perpendicular to the C_{3v} symmetry axis and should correspond to the ν_6 band at ca. 30 meV. The A_2 mode associated to torsional vibrations of ammonium ions with their dipole oriented along the C_{3v} axis should correspond to almost free rotation. Possibly, two bands at the low frequencies of ca. 2.5 and 9 meV, reflect the rotational tunnelling spectrum of NH_4 free rotor states with nuclear spin contributions in the C_{3v} symmetry site. Similarly, a broad distribution of low frequency rotational excitations of NH_4 has been observed in KBr/NH_4Br (0.5%) dilute solution [8]. However, this model was not acceptable to explain the NH_4 rotational tunnelling excitations in the $K_{1-x}(NH_4)_xI$ mixed salts for and $x > 0.15$ and transition energy below 1 meV [3].

It is not doubt that both low frequency bands observed by the IINS spectroscopy in the disorder phase of the $K_{1-x}(NH_4)_xI$ mixed salts correspond to localised dynamics of ammonium ions in crystalline lattice. However, their concentration dependence is even more clear than for higher frequency modes and reflect ammonium-ammonium interactions. This implies that the C_{3v} rotational potential for NH_4 ions directly depends on such interactions. Direct ammonium-ammonium interactions contradict the presentation of this mixed salt as a pure dipolar glass. More detailed studies of the shape, width and intensity of these bands in dependence on concentration and temperature should explain the nature of these interactions and its role in the formation of the orientational glassy state in mixed ammonium salts.

REFERENCES

1. I. Fehst, R. Bohmer, W. Ott, A. Loidl, S. Haussuhl, C. Bostoen, Phys. Rev. Lett., **64** (1990) 3139-3142.
2. J.F.Berret, C.Bostoen, B.Hennion, Phys.Rev., **B46** (1992) 13747-13750.
3. C.Bostoen, G.Coddens, W.Wegener, J.Chem.Phys., **91** (1989) 6337-6345.
4. R.Mukhopadhyay, J.Tomkinson, C.J.Carlile, Europhys.Lett., **17** (1992) 201-206.
5. J.Tomkinson, B.A.Dasannacharya, P.S.Goyal and R.Chakravarthy, J.Chem.Soc.Faraday Trans., **87** (1991) 3431-3433.
6. I. Natkaniec, S.I. Bragin, J. Brankowski, J. Mayer, Proc. ICANS-XII, Abingdon 1993, RAL Report 94-025, Vol. I. p.89-96.
7. G.Dolling, R.A.Cowley. C.Schittenhelm, and I.M.Thorson, Phys. Rev., **147** (1966) 577-582.
8. A. Inaba, H. Chihara, J.A. Morrison, H. Blank, A. Heideman, J. Tomkinson, J. Phys. Soc. Japan, **59** (1990) 522-531.

Investigation of the librational spectrum of deuterated thiocyanate ammonium.

L.S. Smirnov, I. Natkaniec[&], S.I. Bragin

Frank Laboratory of Neutron Physics, JINR, 141980 Dubna, Russia.
&-On leave from H. Niewodniczanski Institute of Nuclear Physics, 31-342 Krakow, Poland

Thiocyanate ammonium, NH_4SCN, undergoes phase transitions from the tetragonal phase I with space group D_{4h}^{18} through the orthorhombic phase II with space group D_{2h}^{11} to the monoclinic phase III with space group C_{2h}^{5} during cooling at 390 and 360K, respectively. The phase transition from the tetragonal phase I to the orthorhombic phase II is due to the ordering of molecular SCN^- ions and the phase transition from the orthorhombic phase II to the monoclinic phase III is due to the ordering of the molecular NH_4^+ ions. The contribution of ammonium ions to the phase transitions of NH_4SCN was investigated with the help of inelastic incoherent neutron scattering in [1]. In this work, the librational spectrum of ammonium was determined.

In order to be sure that energies in the region from 300 to 400 cm^{-1} are indeed librational energies it is necessary to carry out the investigation of ammonium dynamics with inelastic incoherent neutron scattering of deuterated ammonium thiocyanate. It is known that the librational energies of deuterated ammonium decrease by 1.4 times and this method is used to identify rotational states.

In a recent report the results of the inelastic incoherent neutron scattering (IINS) investigation of the deuterated thiocyanate ammonium in the monoclinic phase at 9K are presented. The G(E) vibrational density of state weighted on amplitude of atom vibrations, obtained from the IINS spectra for ND_4SCN and earlier for NH_4SCN [1] are presented in Fig. 1. The optical translational and librational energies determined for deuterated and protonated ammonium are summed in the Table.

Table. Energies of $N(H/D)_4$ (are given in cm^{-1})

Modes	NH_4SCN	ND_4SCN	E(H)/E(D)
ν_5	179	168	1.065
	193	182	1.060
ν_6	318	235	1.353
	351	256	1.371
	380	278	1.366
	409	300	1.363

The obtained relations of E(H)/E(D) for ν_5 and ν_6 are in accordance with the band identification done in [1].

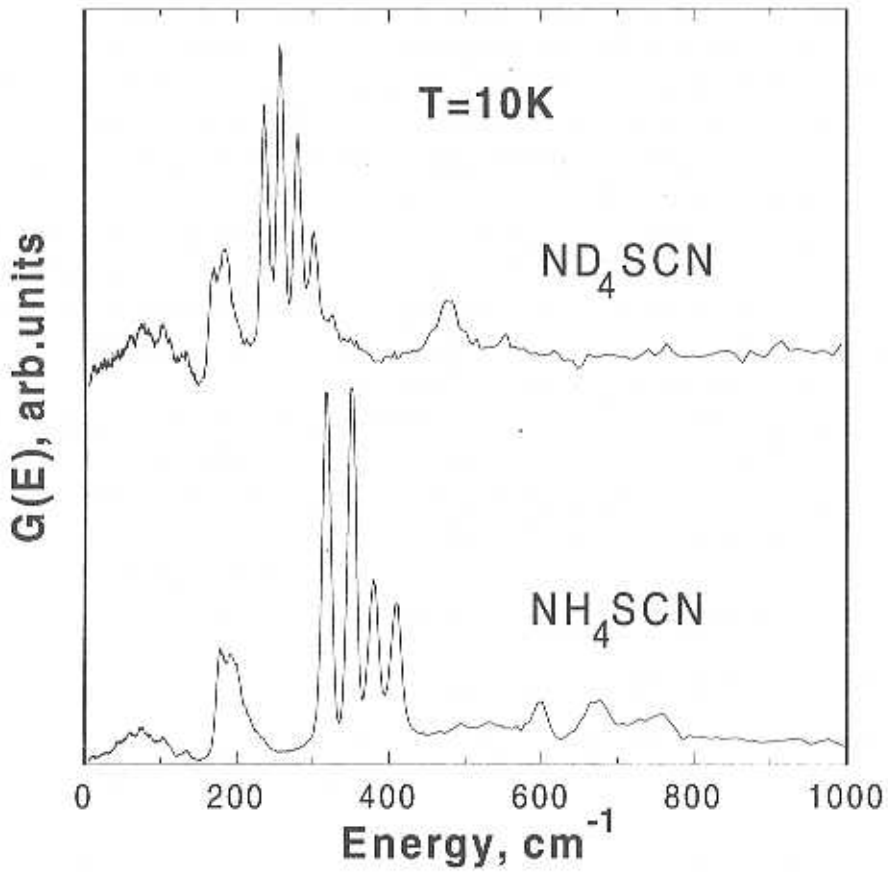

Fig. 1. The comparison of G(E) spectra for NH_4SCN and ND_4SCN at 10 K.

Reference:

1. I. Natkaniec, L.S. Smirnov, A.I. Solov'ev, Physica **B 213&214** (1995) 667-668.

DENSITY OF VIBRATIONAL STATES OF HIGHLY DISPERSE CARBONS.

1. Nanodisperse diamonds

I.Markichev*, E.Sheka*, A.Muzychka** and V.Khavryutchenko**

(*) *Russian Peoples' Friendship University, Moscow*
(**)*LNP, JINR, Dubna*

Nano-size carbons have recently attracted a great attention due to promising perspectives of their large application in science and technology. This is mainly due to a large variety of carbon nanospecies: from nanodiamonds and nanographites compositions to fullerenes. This variety of nanospecies, having sometimes a similar appearance, in its turn, has put a problem of the species identification and sertification. A lot of IR and Raman spectroscopic studied has been undertaken to tackle the problem for the last few years. However, the above optical methods occurred to be unsufficient in some cases. Besides that, optical methods are mainly related to bulk vibrations of the species while the surface and its vibrations play an important role for nanospecies. These facts have necessitated a performance of a series of nanospecies vibrational spectra studies using the technique of inelastic neutron scattering (INS), which has highlighted itself as an appropriate tool for both bulk and surface nanospecies vibrations investigation [1].

Below a series of experiments is presented which was carried out for the following carbon nanospecies:

- nanodisperse diamond of different grain size and of different origin;
- exfoliated graphite;
- graphitized black;
- endogenic carbon dust;
- carbon heterosorbents.

This report presents the results obtained for nanodiamonds. Experiments were carried out on INS spectrometer KDSOG-M at T=80K. Three samples were studied.

Sample 1 was obtained in the course of a blow-driven reaction between trinitritoluene and hexan. It consists of particles with the diameter of 35-40Å in average. According to X-Ray study, the particles have a diamond-like structure. Their surface is partially graphitized. Sample mass is of 39.4 gr, measuring time is 5 hours. The sample was provided by Physical Department of the Moscow State University.

Samples 2 and 3 are commersial syntethic diamonds produced in the Institute of superhard materials of the national Ac.Sci. of the Ukraine. They differ by the average grain size which is of 60-40 mcm for sample 2 (it will be called below as a macrodiamond) and is much less for sample 3, corresponding to the specific area value

of 187 m^2/gr. The both samples masses are of 20 and 19 gr, respectively. Measuring time was 8 hours in both cases.

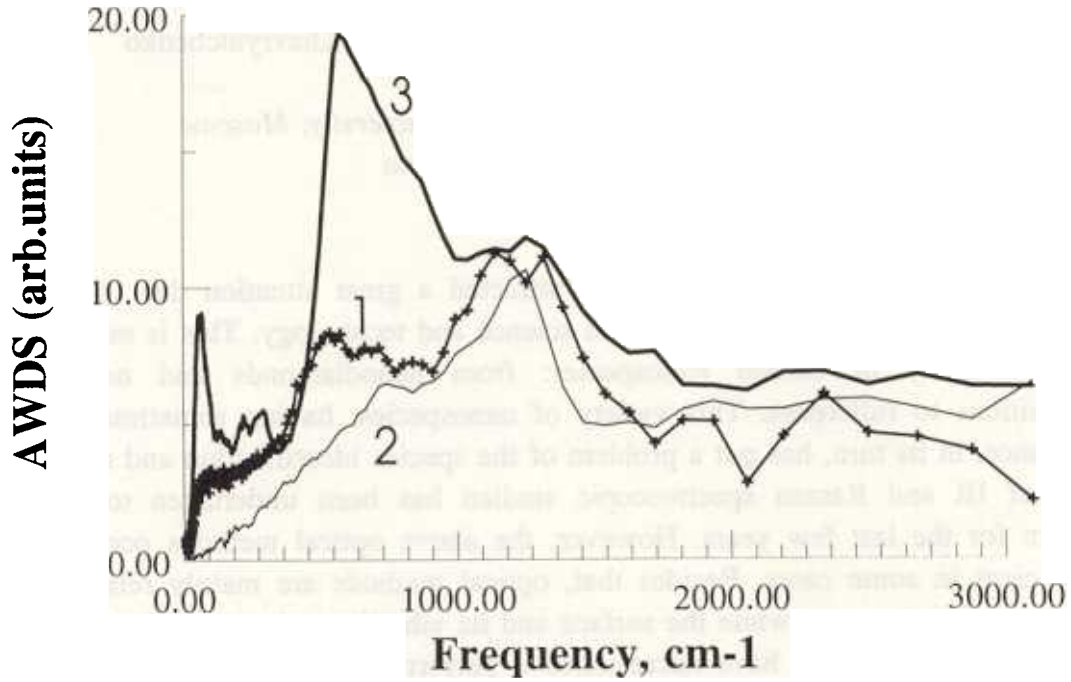

Fig.1

Fig.1 presents the sample spectra of double-amplitude weighted density of vibrational states (AWDS) normalized per 100 gr of mass and 1 hour of measuring time. The spectra numbering in Fig.1 corresponds to the sample numbering. As expected, the spectrum of macrodiamond (sample 2) is of the lowest intensity among the spectra set. This is due to the fact that this spectrum corresponds to bulk vibrations only while the other two spectra, related to more disperse species, are composed of both bulk and surface vibrations. In the latter case the vibrations of the surface zone as whole are implied. Spectrum 2 fits well the DOS of bulk vibrational states for diamond [2]. Its shape has a peculiar two-hump structure with maxima positioned at 700 and 1200-1250 cm-1. A sharp decreasing of the spectrum intensity is observed over 1300 cm-1.

To analyse spectra 1 and 3 means to decompose them into the spectra of their constituents, primarily into spectra of bulk and surface vibrations. To obtain the atter spectra, it is necessary to substract spectrum 2 which presents the spectrum of the bulk modes, from spectra 1 and 3. Fig.2. shows a residual spectrum (3) - (2). The spectrum (1) - (2) has the same shape but is less by intensity. The residual spectrum in Fig.2 in the main spectral region up to 1200 cm-1 is fully similar to a well known spectrum of a quenched water (see, for example, [1]) so that it should be attributed to a confined water in the body of both nanodiamond powders. Further investigation should answer

a question what kind of nano-scale porous or capilar structure is responsible for catching water inside the powder of nanodiamonds.

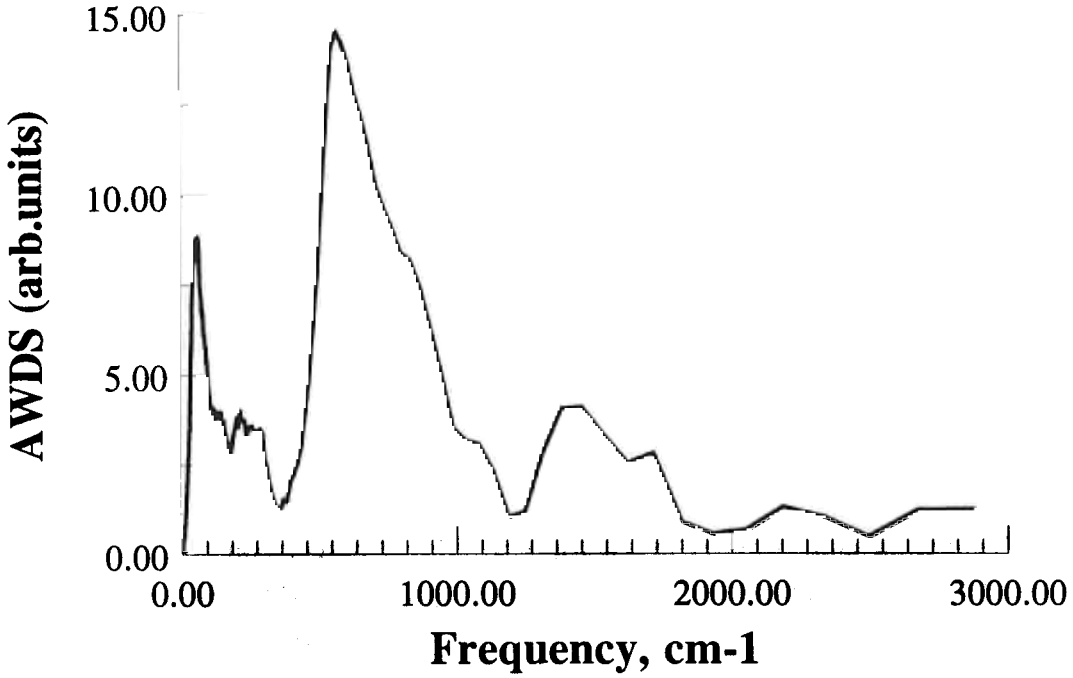

Fig.2

1. E.F.Sheka, V.D.Khavryutchenko and I.V.Markichev, Russian Chemical Reviews, 64 (5), 389-414 (1995)

2. P.Pavone, K.Karch, O.Schutt, W.Windl, D.Strauch, P.Gianozzi and S.Baroni, Phys.Rev.B48, 3156 (1993).

The Interaction of Oxygen (Nitrogen) with Hydrogen in Ti, V and Ta.

V.V.Sumin, Ch.Gantulga

LNP, JINR, Dubna, Russia

The fast ion channelling (FIC) showed than hydrogen mores from tetrahedral positions to the octahedral in V-O-H solid solution (SS) or low symmetrical positions in Ta-N SS. [1] due to O(N)-H interaction.

So oxygen or nitrogen locate in the octahedral positions the FIC method can not determine exactly the hydrogen location.We check these statements by INS.

Sample preparations. The vanadium was alloyed by the ultimate concentration of oxygen α-phase (6 at%). The sample was charged by hydrogen at 800^0C and water quenched.

One tantalum sample was alloyed preliminary by 3 at% of vanadium and then saturated by nitrogen and hydrogen from the gas phase and water quenched from 800^0C. Vanadium and nitrogen in Ta form additional defect complex, which captures hydrogen. Titanium sample was prepared by melting Ti with TiN to concentration $TiN_{0.05}$ and charged by H. All the samples was single phase as was determined by neutronography.

V - O - H system

In this system the formation of β–V_2H hydride was studied by INS. Due to high luminosity of the KDSOG-2M local mode of hydrogen in the octahedral sites can be measured during 1 hour. So the process of β- V_2H formation was studied at gradual cooling of the samples from room temperature to 210^0K (Fig.1,2). Oxygen courses the substantial influence on this process first of all, the LM energies change by different lows (Fig.3).

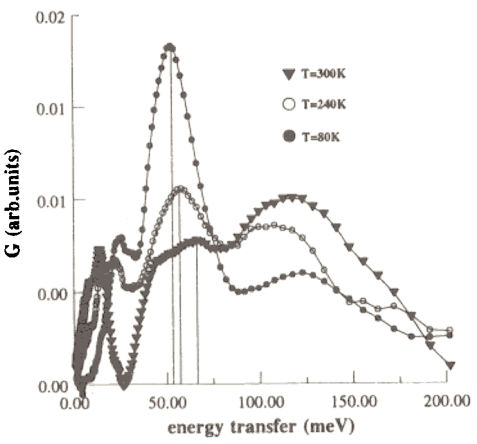

Fig.1 The partial hydrogen function of state (PHFS) in VO H at 300K, 240K and 80K

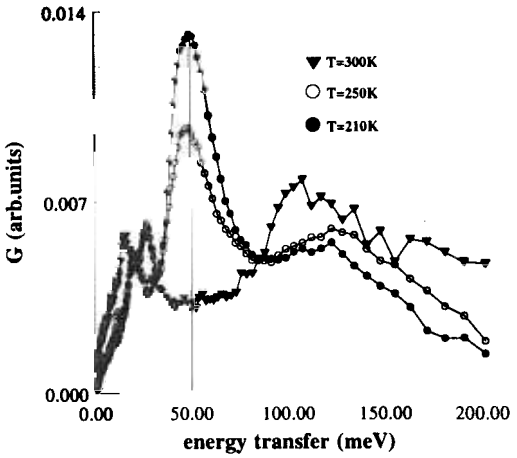

Fig.2 The PHFS in $VH_{0.01}$ at 300K, 250K and 210K

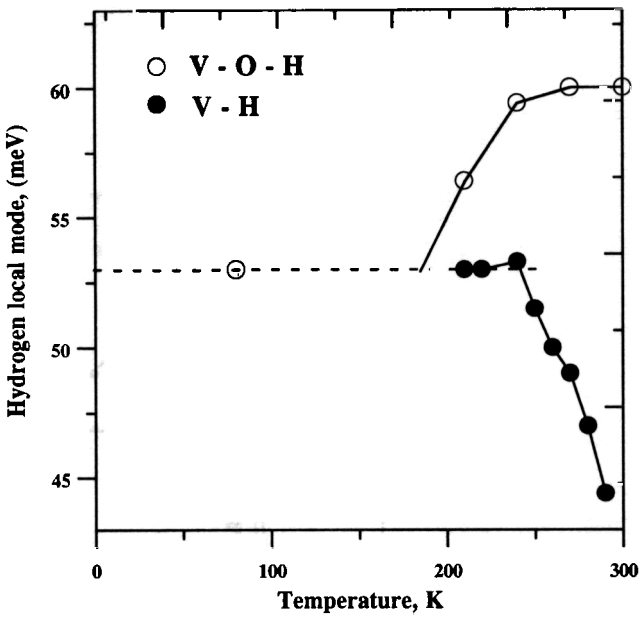

Fig.3 The dependence of LMP versus temperature for the $VO_{0.06}H_{0.03}$ (open circle) and $VH_{0.01}$ (dark circle).

In binary $VH_{0.01}$ system the hydrogen local mode positions (LMP) increase from 45 meV at room temperature to 53 meV at 240^0K and stay constant at more lower temperature. According to [2] hydrogen precipitates into hydride at 260^0K for 1 at% concentration in V. Before this temperature LMP changes can be explained by the preparation of hydrogen atoms to phase transition. This process accompanies by grows of the tetragonality VH_x SS [3]. Fukai [3] proposed that 1T→4T(O) transition perponsed for this tetragonality. We confirm this proposal by INS.

In the case of ternary $VO_{0.06}H_{0.03}$ system, LMP's decries from 63 meV to 53 meV (Fig.3). Oxygen keep hydrogen in SS down to 190^0K. That is on 50^0K lower than for binary V-H system in spite of the greater H concentration in ternary SS.

Both for binary or ternary systems hydrogen takes participation not only in LM but in resonance - like lattice vibrations (RLLV) (Fig.1,2). The positions of this RLLV depend on temperature and close to the predict value 16 meV [4].

$TaN_{0.02}H_{0.045}$ and $TaV_{0.03}N_{0.02}H_{0.02}$ solid solutions.

The binary $TaH_{0.045}$ SS changes essentially the LMP at low temperature due to formation of β-TaH hydride (Fig.4).

In contrary to that the nitrogen contained alloys do not change the LMP at low temperatures (Fig.5,6). From these facts we conclude that N-H or V-N-H interactions keeps hydrogen in SS.

Moreover in $TaV_{0.03}N_{0.02}H_{0.02}$ alloy the hydrogen LM split into three peaks as for ε-V_2H hydride. The model calculation for microcrystal showed that such split can be explained by N-H or H-H interactions throw the deformation fields.

Increasing of deformation fields for nitrogen in Ti with comparison to the fields in Ti-O SS causes the increase the amount of residual hydrogen in octahedral sites of Ti-N SS (Fig.7, peak at 90 meV). So in Ti-N SS this amount is nearly 25%, but for the Ti-O SS it is 7% only [5]. The most part of hydrogen both in the Ti-N and Ti-O SS is in the hydride phases (Fig.8, peak at 153 meV).

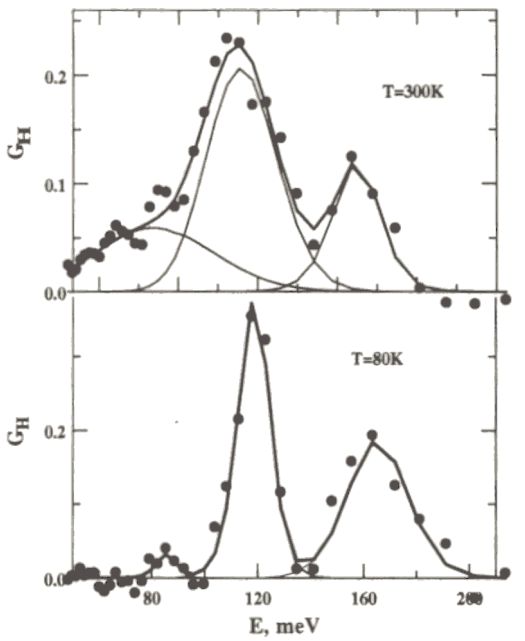

Fig.4 The PHFS in $TaH_{0.045}$ at 300K and 80K

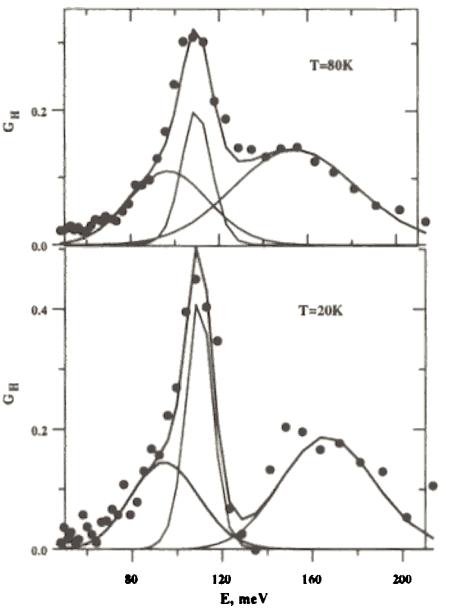

***Fig.5** The PHES in $TaV_{0.03}N_{0.02}H_{0.02}$ at 80K and 20K*

***Fig.6** The PHFS in $TaN_{0.02}H_{0.045}$ at 300K, 80K and 20K*

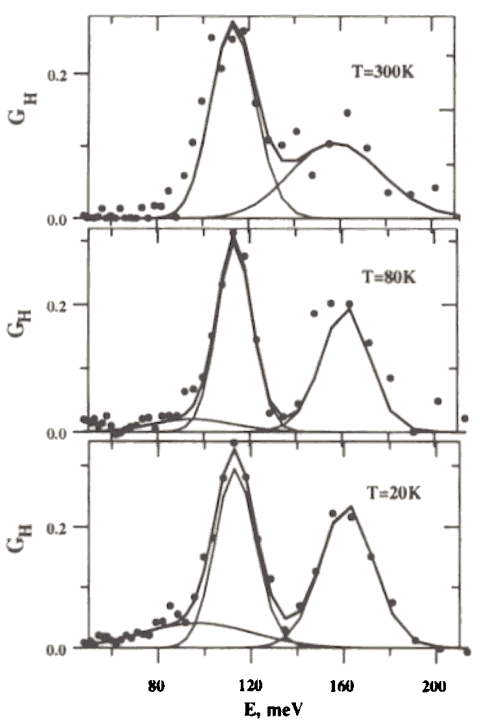

***Fig.7** The PHFS in Ti-N ss at 300K, 210K, and 80K*

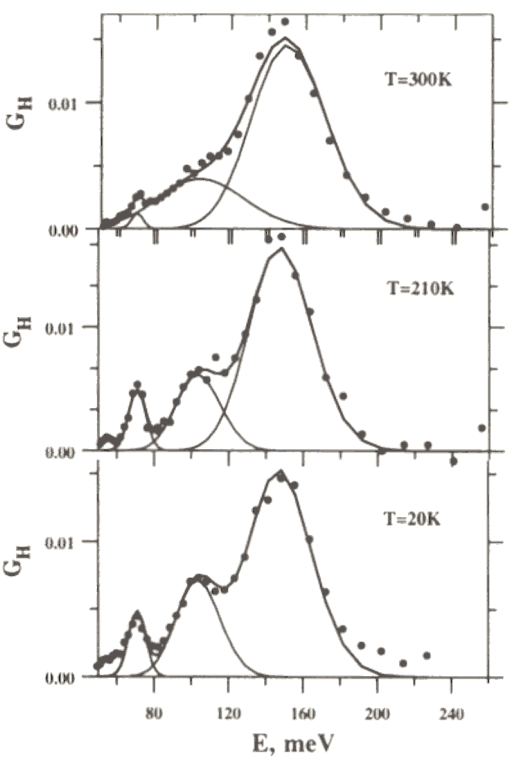

. Literature.

1. Carstanjen H.D., Interstitial Positions and Vibrational Amplitudes of Hydrogen in Metals Investigated by Fast Ion Channelling. Phys.Stat.Sol. (a), 1980, 59, p11-25
2. Hydrogen in Metals, Springer-Verlag, 1978, v2, p51.
3. Suqimoto H. and Fukai Y., Theory of Light Interstitials in BCC Metals, Phys.Rev.B, 1980, v22, p670-680.
4. Schober H.R., Lottner V., Lattice Dynamical Aspects of H in V, Nb, Ta and Pd., Z.Phys.Chemie New Folge, 1979, v114, p203-212.
5. Belushkin A.V., Morozov S.I., Natkanec I., Sumin V.V., Study of the Hydrogen Vibration spectra in Ti-O solid solution by INS. Rapid Communications of JINR, P14-86-41, Dubna, 1986, p8

The $S(q)$ Structural Factor of Liquid ^{4}He for Small q

Zh.A.Kozlov

Frank Laboratory of Neutron Physics, JINR, Dubna, Russia

Bijl [1], Feynmann [2], and Pitayevskii [3] obtained the following expression for $S(q)$ at small wave vectors q and $T \to 0$

$$S(q) = \frac{\hbar q}{2Mc} \qquad (1)$$

under the assumption that only one-photon processes contribute to the $S(q)$ structural factor of liquid ^{4}He. At $T \neq 0$, $S(0) = \rho k_B T K_T$ [4], where ρ is the density of ^{4}He atoms, k_B is Boltzman's constant, and K_T is the isothermic compressibility.

To verify the validity of expression (1), we did the following. Data on integral intensities at T=0.42; 1.45; 2.05, and 2.21 K in [5,6] was obtained by summing all of the neutron scattering components measured in [5, 6]. The heating part of the scattering law was accounted for using a detail equilibrium relation. The phonon regions of these data for $q \approx (0{,}1 \div 0{,}6)$ Å^{-1} were described by two functions:

$$Z_1(q) = a_1 + a_2 q,$$

$$Z_2(q) = b_1 + b_2 q + b_3 q^2,$$

where a_i and b_i are constants. Statistical criteria for the approximation precision χ_1^2 were obtained. Then, the temperature dependence for the so-called variance ratio $v^2 = \chi_1^2/\chi_2^2$. was built. The variance ratio characterizes the deviation degree of experimental data from a straight line.. Figures 1 a, b illustrate the dependencies of the integral intensities on the phase vectors and the description of phonon areas using a straight line for T=0.42 K and a curved line for T=2.21 K. Figure 1 c shows the dependence of v^2 on T. The equality $v^2=1$ means that experimental data on S(q) can be described unambiguously using a straight line. As is seen from Fig. 1, at increasing of temperature below the λ-point, sufficiently smooth bending of the curve changes for a sharp jump at the phase transition point T_λ. The circle at T=0 K was drawn from theoretical considerations.

As a result, we can state that in the phonon region, the dependence of the statistical structural factor on the wave vector of liquid ^{4}He smoothly tends to a straight line at decreasing temperature. At the same time, the intensity of inelastic neutron scattering has a tendency to decrease to zero at a decrease in the temperature and wave vector. Note that elastic scattering is not observed in the scattering of neutrons in superfluid ^{4}He. Thus, dependence (1) was experimentally confirmed.

References

1. Bijl A.- Physica, 1940, vol.7, p.869.
2. Feynman R.P.- Phys. Rev., 1954, vol.94, p.262.
3. Pitaevskii L. P.- ZhETF, 1956, vol.31, p.536 (in Russian).
4. Price P.J.- Phys. Rev., 1954, vol.94, p.257.
5. Blagoveshchenskii N.M., Bogoyavlenskii I.V., Karnatsevich L.V., Kozlov Zh.A., Kolobrodov V.G., Priezzhev V.B., Puchkov A.V., Skomorokhov A.N., Yarunin V.S.- Phys. Rev. B, 1994, vol.50, p.16550-16565; Preprint JINR P3-94-125, Dubna, 1994 (in Russian).
6. Kozlov Zh. A., Russian J. Particle and Nucleus, 1996, v.6 (in Russian).

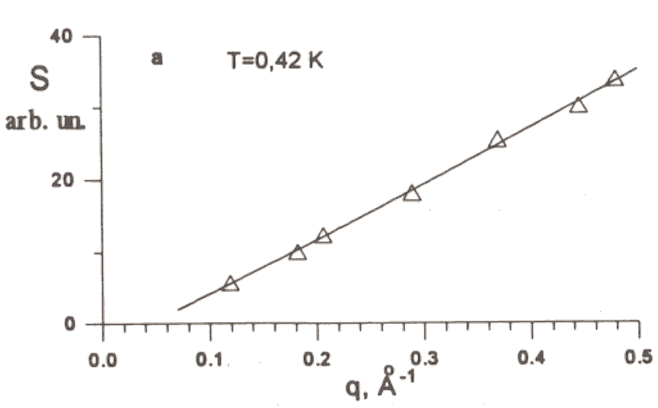

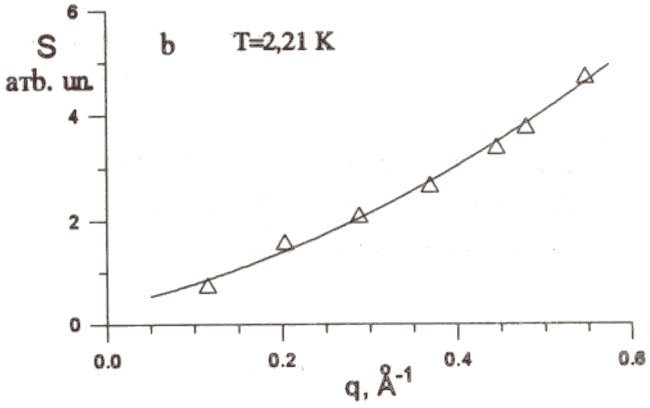

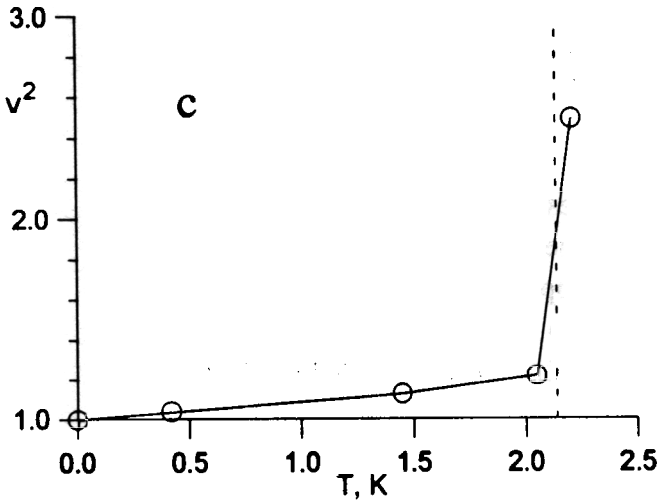

Fig. 1. a, b. The dependencies of the integral intensities on q for T=0.42 and 2.21 K, and the curves which describe the phonon region. c. The dependence of v^2 on T.

Study of depth profiles of elements of thin layer structures using RBS technique

Kobzev A.P., Korneev D.A., Nikonov O.A.(JINR)
Ul'yanov V.A., Peskov B.G., Pleshanov N.K., Pusenkov V.M., Siber E.V.,
Soroko Z.N., Syromyatnikov V.G., Schebetov A.F.(PNPI, Gatchina)

At the present time polarizing devices on the basis of supermirrors are widely used to obtain neutron polarized beams. Supermirrors represent aperiodic multilayered structures of alternating magnetic and nonmagnetic layer structures with the thickness changing according to the appropriate law from 75 A to 700A. To produce highly effective polarizing supermirrors, it is necessary to select the elementary composition of FeCo/TiZr, Co/Ti layers in such a way that the difference between a nuclear and magnetic potential should be equal to a nuclear potential of nonmagnetic ones. The layers themselves and their boundaries are not ideal due to roughness and mixture of materials at the boundaries as they are being deposited, as well as different kinds of admixtures appear (O, Ar, C, N and others). Moreover, while the polarizing devices are in use in real conditions, oxidation of the upper layer takes place which worsens the polarizing properties of mirrors too.

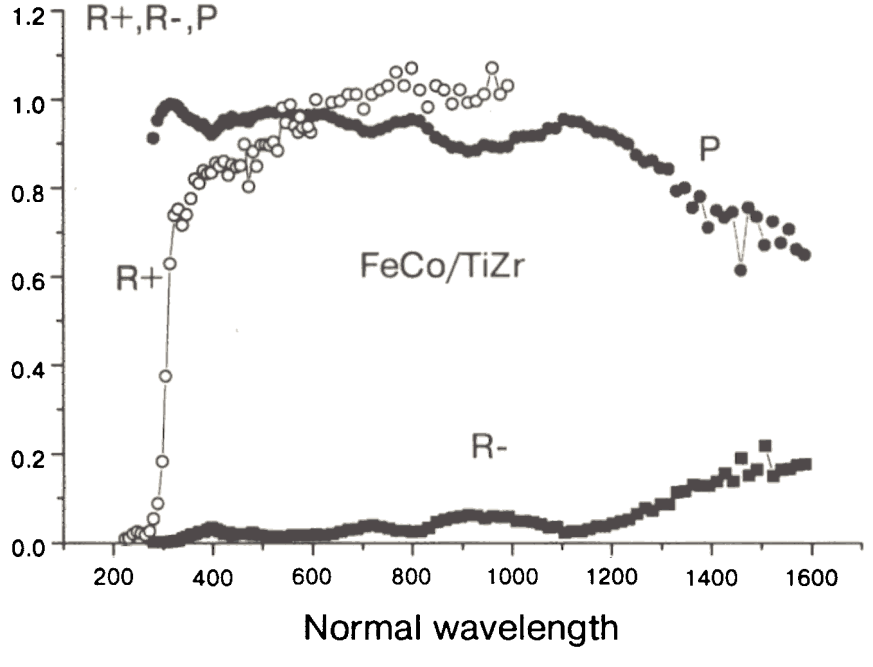

Fig.1. Reflection coefficients for two spin components and polarizing capability of supermirror.

As an example, Fig.1 shows the reflection curves for the two spin components R^+,R^- and the polarizing efficiency of a supermirror with the layers FeCo/TiZr. One can see that the polarizing efficiency of a mirror has gaps which are probably connected with the imperfection of the element composition of layers reflecting neutrons with λ =400-700A. These data have been obtained at the reflectometer at the WWR-M reactor in Gatchina.

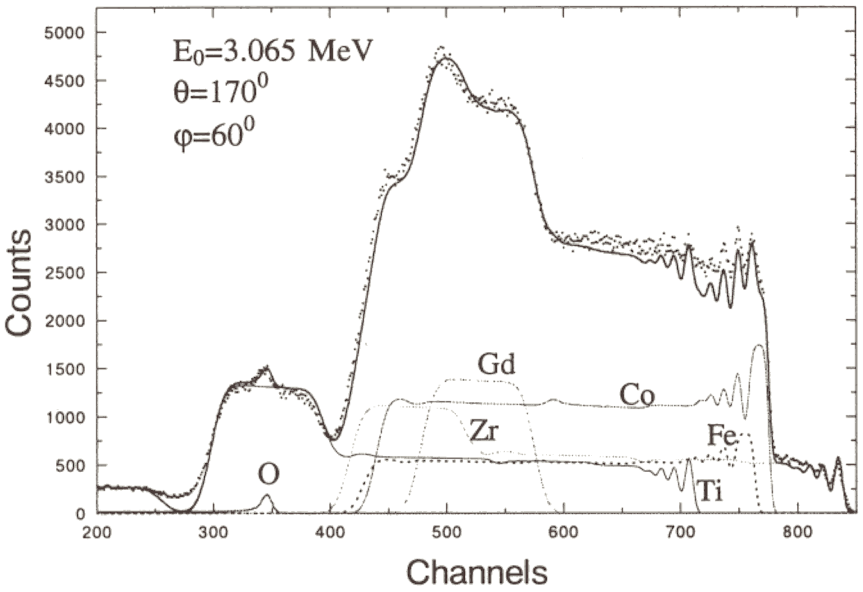

Fig.2. Experimental and calculated spectra of scattered ions $^4He^+$ for supermirror.

Depth profiles of elements in multilayered structures have been studied using the RBS technique at the electrostatic generator EG-5 FLNF. Fig.2 shows one of the experimental spectra, partial spectra of all elements involved in the composition of different mirror layers, as well as the resulting spectrum calculated for an appropriate model. The calculated spectrum has been obtained as a result of the variation of model parameters (composition and layer thickness) up to the achievement of the best description of the experimental spectrum. The peak in Fig. 2, corresponding to the resonance scattering of helium ions on oxygen, shows its composition in the first layer of the multilayer structure. The spectra at higher energies have been measured to analyse the following layers. As it has been seen, a sample can be analysed at its whole depth up to the substratum (glass). Changing experimental conditions, one can achieve the resolution in tens of angstroms, i. e. to observe separate layers.

Thus using the non-destructive technique one can obtain a full depth profile of all main and admixed elements in the composition of multilayered structures. The obtained results permit us to understand the reasons of imperfection of polarized neutrons and to introduce some changes in the manufacturing process.

Off-specular Neutron Reflection from Magnetic Media with Nondiagonal Reflectivity Matrices

Dmitri A. Korneev[1], Victor I. Bodnarchuk[1], Vladimir K. Ignatovich[2]
[1]*Laboratory of neutron physics, JINR, 141980 Dubna Moscow reg., Russia*
[2]*Research Reactor Institute Kyoto University Kumatori-cho, Senan-gan, Osaka 590-04, Japan.*
(Received February 1, 1996)

The reflection of neutrons from magnetic substances is described using the reflection matrix with nondiagonal, in general, matrix elements which determine neutron spin reverse. In external field the spin reverse is accompanied by changes of the neutron kinetic energy and reflection angle. The particular case of reflection from a magnetic mirror with magnetization noncollinear to the external field is considered. The probability of spin reverse and a deviation of reflection angles from the specular one are calculated. The experiment to observe this effect is described and its results are reported.

KEYWORDS: thermal neutrons, magnetic scattering, polarization, optical potential

§1. Introduction

Since the time of the first works by Hughes and Burgy[1)] specular reflection has been used to polarize neutrons. With polarized neutrons one can investigate, for instance, magnetization profiles of films and multilayered systems[2-6)]. It was pointed out[7-13)] that reflection from films with noncollinear magnetic structures is more complicated than reflection from films with collinear ones. In noncollinear case the reflection is characterized by the reflection matrix:

$$\hat{R} = \begin{pmatrix} R_{++} & R_{+-} \\ R_{-+} & R_{--} \end{pmatrix}$$

with nonzero elements R_{+-} and R_{-+}. To measure all matrix elements in $\hat{R}$ is the main goal of polarized neutron reflectometry.

In the next section, the angular characteristics of reflection with spin-flip in external fields are considered. In the third section, the matrix elements of $\hat{R}$ and the intensities of constituent beams for the case of reflection from a magnetic mirror with magnetization noncollinear to the external field are calculated. In the fourth section, the experiment to observe the off-specular reflection is described

§2. Angular splitting of the reflected beam

The reflection of neutrons from an interface in an external magnetic field can be off-specular (though coherent) if it is accompanied by spin flipping[7,9)]. In general, the incident beam after reflection undergoes triple splitting, as shown in fig. 1. It contains the middle part which is specular and two side lobes which are off-specular and perfectly polarized. The intensity of the side lobes are determined by the matrix elements R_{+-} and R_{-+} of the matrix $\hat{R}$ and by incident beam polarization. If the incident beam is perfectly polarized, one of the side lobes vanishes. If the incident beam is nonpolarized, two side beams in weak external fields have almost equal intensities. The splitting of the beam takes place because of spin flipping, energy conservation and the conservation the of components of neutron momentum parallel to the interface.

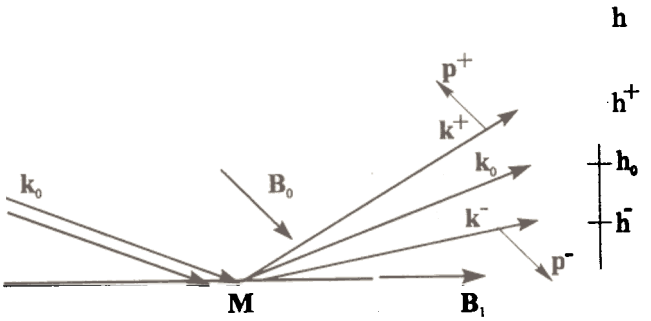

Fig. 1. Following the reflection from a magnetized mirror with the magnetization **M** noncollinear to the external magnetic field $\mathbf{B}_0$ the nonpolarized incident neutron beam with a wave vector k_0 splits into three beams. Two off-specular beams with the wave vectors k^+ and k^- are ideally polarized. The splitting of the beam gives the distribution over height h of the reflected neutrons and it can be measured by a moving or a position sensitive detector.

Let us denote $\mathbf{k}=(\mathbf{k}_\parallel, \mathbf{k}_\perp)$ the wave vector of the incident neutron with the $\mathbf{k}_\perp$, $\mathbf{k}_\parallel$ being its normal and parallel to the surface components. In the external field **B** the neutron has the potential energy $-\sigma\mathbf{B}$, where **B** is measured in $\hbar^2/2m\mu$ (m, μ are the neutron mass and magnetic moment, respectively) and σ are the Pauli matrices. On spin reverse the potential energy changes in magnitude by ①2B. Because of energy conservation it changes the kinetic energy: $k^2 \to k^2$①2B. In the reflection from an interface the components $\mathbf{k}_\parallel$, are also conserved. Thus the change of the kinetic energy means the change in the normal component $\mathbf{k}_\perp$: $k_\perp \to k_\perp^\pm = \sqrt{k_\perp^2 \pm 2B}$, and as a result to change in the reflection angle. It is not difficult to calculate the angular deviation of shifted beams. For a small grazing angle $\phi_0=10^{-2}\div10^{-3}$ we have

$$\frac{\Delta\phi^\pm}{\phi_0} = \frac{\Delta k^\pm_\perp}{k_\perp} = \sqrt{1 \pm 2B/k^2} - 1$$
$$= \sqrt{1 \pm 1.47\cdot10^{-10} B_0 \lambda^2/\phi_0^2} - 1$$

Here the neutron wavelength λ is measured in Angstroms, B in Gauss, and ϕ_0 in radians.

The dependence of relative splitting $\Delta\phi^\pm/\phi_0$ on λ and B is shown in fig.2.

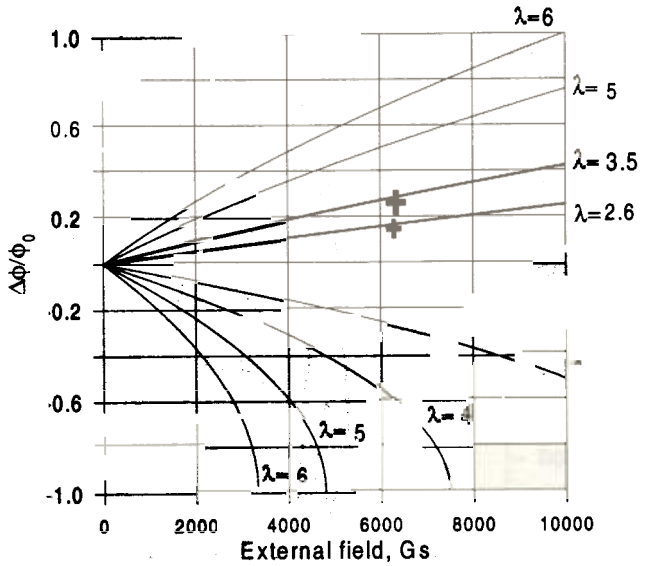

Fig.2. The relative angular splitting of spin reversed beams in dependence on λ (in Angstroms) and the external magnetic field for ϕ_0=4.2mrd. The crosses are the experimental points (see sec. 4).

If the external field is sufficiently large, spin reverse is forbidden for $\Delta\phi<0$.

§3. Matrix $\hat{R}$

Let us find the solution of the Schrödinger equation in presence of the external magnetic field $\mathbf{B}_0$ and a magnetized reflecting mirror:

$$(\Delta - u\theta(z>0) + \sigma\mathbf{B}(z) + k^2)\psi = 0$$

where u is an optical potential of the mirror, which is supposed to fill the half space z > 0, θ is a step function equal to unity when the unequality in its argument is satisfied and to zero in the opposite case,

$$\mathbf{B}(z) = \mathbf{B}_0\theta(z<0) + \mathbf{B}_1\theta(z>0),$$

and $\mathbf{B}_1$ is the magnetic induction of the mirror. We consider the case when $\mathbf{B}_0$ unparallel to $\mathbf{B}_1$. The solution is: $\psi(\mathbf{r}) = \exp(i\mathbf{k}_1\mathbf{r}_1)\xi(z)$, where

$$\xi(z) = \theta(z<0)[\exp(i\hat{k}_\perp^+ z)\xi_0 + \exp(-i\hat{k}_\perp^+ z)\hat{R}\xi_0] + \theta(z<0)\exp(i\hat{k}'^+_\perp z)\hat{T}\xi_0$$

$\hat{R}$, $\hat{T}$ are reflection and transmission matrices, $\hat{k}_\perp^\pm = \sqrt{k_\perp^2 \pm \sigma B}$, $\hat{k}'^\pm_\perp = \sqrt{k_\perp^2 - u \pm \sigma B}$, and ξ is the spinor state of the incident particle. For simplicity in the following, we shall omit the subscript ⊥.

Matching of the wave function at the interface z=0 for arbitrary ξ_0 gives two equations for $\hat{R}$ and $\hat{T}$:

$$\hat{I} + \hat{R} = \hat{T},\ \hat{k}^+(\hat{I} - \hat{R}) = \hat{k}'^+.$$

The solution of these equations can be represented as follows:

$$\hat{R} = (\hat{k}^+ + \hat{k}'^+)^{-1}(\hat{k}^+ - \hat{k}'^+),\ \hat{T} = (\hat{k}^+ + \hat{k}'^+)^{-1}2\hat{k}^+$$

Here we shall consider in details only the matrix $\hat{R}$.

It is possible to get rid of the matrices σ in the denominator by representing $\hat{R}$ in the form

$$\hat{R} = (\hat{k}^- + \hat{k}'^-)(\hat{k}^+ - \hat{k}'^+)/N \equiv \hat{A}/N$$

where, N is the number and it is useful to calculate it as a matrix element:

$$N = \langle + | k^+k^- + \hat{k}'^+\hat{k}'^- + \hat{k}'^- k^+ + k^-\hat{k}'^+ | + \rangle,$$

where $|\pm\rangle$ represent the eigen states of the matrix $\sigma\mathbf{B}_0$:

$$\sigma\mathbf{B}_0|\pm\rangle = \pm B_0|\pm\rangle.$$

Evaluation gives

$$N = (k^+ + k'^+)(k^- + k'^-) - (k'^- - k'^+)(k^+ - k^-)\sin^2(\chi/2)$$

where $k^\pm = \sqrt{k^2 \pm B_0}$ and $k'^\pm = \sqrt{k^2 - u \pm B_1}$ are the c-numbers now, and χ is the angle between vectors $\mathbf{B}_0$ and $\mathbf{B}_1$. The numerator of (3.2) can be reduced to the form:

$$\hat{A} = k^-k^+ - k'^-k'^+ + \hat{k}^-\hat{k}'^+ - \hat{k}'^-\hat{k}^+ =$$
$$= k^+k^- - k'^+k'^- + (1/2)(k'^- + k'^+)(\hat{k}^+ - \hat{k}^-)$$
$$-(1/2)(k'^+ - k'^-)(\hat{k}^-\sigma\mathbf{b}_1 + \sigma\mathbf{b}_1\hat{k}^+)$$

where the first two terms do not contain the σ matrices at all, and $\mathbf{b}_1$ is the unit vector in the direction of $\mathbf{B}_1$.

Now we are calculate matrix elements of $\hat{A}$

$$\langle\pm|\hat{A}|\pm\rangle = (k^- \pm k'^-)(k^+ \mp k'^+) \pm (k'^+ - k'^-)(k^+ + k^-)\sin^2(\chi/2),$$

$$\langle\mp|\hat{A}|\pm\rangle = -(k'^+ - k'^-)k^\pm \sin\chi,$$

In the case of χ=0 (and the similary for χ=π) the matrix $\hat{R}$ becomes diagonal with the elements:

$$R_+ = (k^+ - k'^+)/(k^+ + k'^+),\quad R_- = (k^- - k'^-)/(k^- + k'^-)$$

For the general case the final expressions for the matrix elements of $\hat{R}$ are:

$$R_{\pm\pm} = \frac{1}{C}\left\{R_\pm \mp \frac{(k'^+ - k'^-)(k^+ + k^-)}{(k^- + k'^-)(k^+ + k'^+)}\sin^2(\chi/2)\right\}$$

$$R_{\pm\mp} = \frac{1}{C}\left\{\frac{(k'^+ - k'^-)k^\mp}{(k^- + k'^+)(k^+ + k'^+)}\sin\chi\right\}$$

$$C = 1 - \frac{(k'^+ - k'^-)(k^- - k^+)}{(k^- + k'^-)(k^+ + k'^+)}\sin^2(\chi/2).$$

These formulas are useful to calculate the beam splitting, but the notations are not appropriate for an experimerit, becuase both spin states in the incident beam are characterized by the sam wave vector $\mathbf{k}^+ = \mathbf{k}^- = \mathbf{k}$ with a given normal component k. Thus, if we consider the splitting of the part of the beam initially polarized along the field, we must replace k^2-B_0 by k^2 which means shifting of all k^2 in (3.5) by $+B_0$. Thus, $\mathbf{k}^+$ for that part of the beam becomes, $k^+ = \sqrt{k^2 + 2B_0}$, and $k'^\pm = \sqrt{k^2 - u \pm (B_1 \pm B_0)}$. For the part of the incident beam polarized in the opposite direction we must take $k^+ \equiv k$ and then, $k^- = \sqrt{k^2 - 2B_0}$, and $k'^\pm = \sqrt{k^2 - u \pm (B_1 \mp B_0)}$.

It is easy to estimate the intensity of reflected beams in the case when the inside field is strong enough to make k'^- be imaginary, and leave k'^+ to be real. In the first

approxirnation with respect to B_0/k^2 the denominator can be replaced by 1, and the intetisity of the off-specular beam become proportional to

$$|R_{-+}|^2 = k^2\left|\frac{-(k'^- - k'^+)}{(k^+ + k'^+)(k^- + k'^-)}\sin\chi\right|^2 = \frac{\gamma B_1 \sin^2\chi}{2(u+B_1)},$$

where $\gamma=|2k/(k+k'^+)|^2\approx 1$.

§4. Experiment

The experiment was performed at the time-of-flight reflectometer of polarized neutrons at the IBR-2 reactor in Dubna.

The sample was a thin anizotropic FeCo film on a glass substrate. The external field was applied either parallel to the anizotropy axis in the film plane ($\chi=0$) or at an angle of 76deg. to it (out of plane). The magnitude of the external field could be varied in the range 0.01÷7kGs. The polarized neutron beam with a wide Maxwellian spectrum was incident on the film at a grazing angle ϕ_0=4.2mrd. The polarization of the beam P(λ) was a monotonous function decreasing from P=0.98 at λ=1.8Å to P=0.5 at λ=7Å. The detector with a cadmium slit of 0.5mm width was placed at 2.68m from the sample. Thus, the angular aperture of the detector was $\delta\phi$=0.18mrd. To determine the reflection coefficients the intensity of the incident and reflected neutrons were measured at different orientation and magnitudes of the external field B.

For $\chi=0$ the dependence of $N_+R_{++}+N_-R_{-+}$ on the wavelength was measured. Here $N_\pm(\lambda)$ are proportional to the intensities of the incident neutrons with two spin projections on the external field, and $R_\pm$ are the squares of modules of the related reflection amplitudes.

For χ=76deg., the angular distributions of the reflected neutrons were measured for two magnitudes of the external field: 0.2 and 6.3kGs. (fig.3). In the field H=6.3kGs, off-specular neutrons were observed at $\phi>\phi_0$. To determine the dependence of $\Delta\phi=\phi-\phi_0$ on λ the energy range of counted neutrons was restricted to two intervals $\Delta\lambda_1$ and $\Delta\lambda_2$ around λ_1=2.6Å and λ_2=3.5Å respectively. The measured ratio of the magnitudes $\Delta\phi_1(\lambda_1)$ and $\Delta\phi_2(\lambda_2)$ (fig.3b) satisfies the relation $\Delta\phi_1(\lambda_1)/\Delta\phi_2(\lambda_2)=(\lambda_1/\lambda_2)^2$ with the precision better than 5%, and corroborates the quadratic dependence of $\Delta\phi$ on λ. The measurements of $\Delta\phi$ at fixed λ and different B corroborate the linear dependence $\Delta\phi\propto B$.

For the fixed position of the detector at $\Delta\phi$=0.7mrd and two magnitudes of the external field: B=6.3 and 3.2kGs the spectral dependence of the square modules of R_{++}, R_{+-}, and R_{-+} were measured (fig. 4). The spectral interval of the measurments was determined by the angular detector aperture $\delta\phi$=0.18mrd.

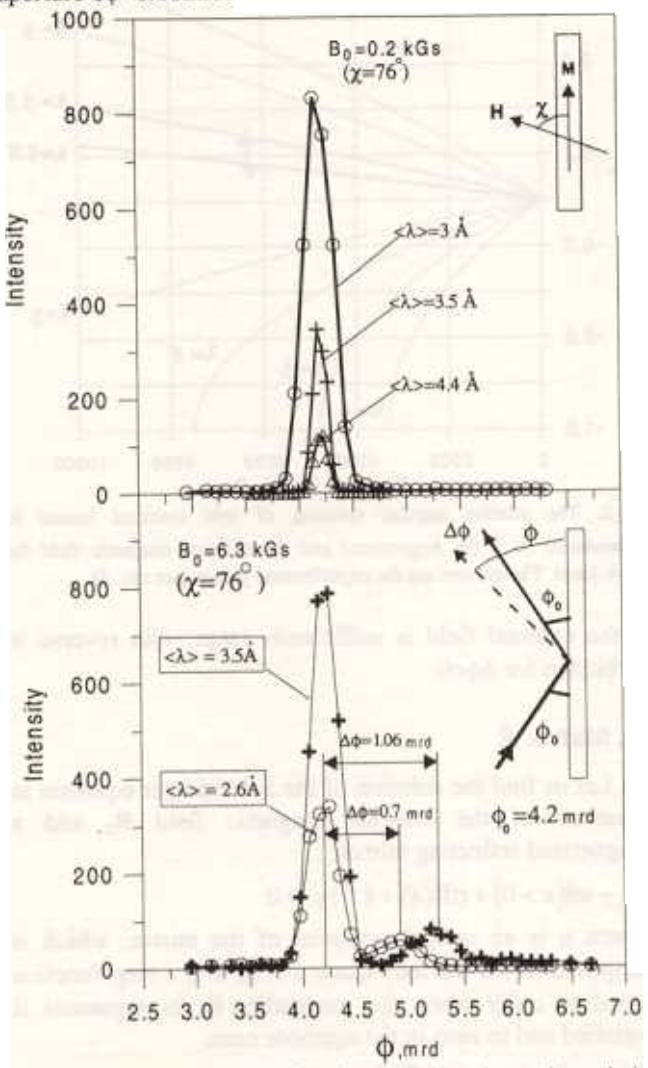

Fig.3. The dependence of the reflected neutron intensity on the angle ϕ of detector positioning.
a) B=0.2kGs, χ=76°, the detector aperture $\delta\phi$=0.18mrd, the grazing angle of the incident beam is ϕ_0=4.2mrd. The intensitydistribution maximums for different λ are observed at the same specular angle $\phi=\phi_0$.
b) B=6.3kGs, χ=76°, $\delta\phi$=0.18mrd , ϕ_0=4.2mrd. The angular distribution of the reflected intensity for two different intervals of λ. In the vicinity of the specular beam($\phi=\phi_0$), off-specular ones appear. The angular shift $\Delta\phi=\phi-\phi_0$ has the quadratic dependence on averaged wavelength $<\lambda>$.

The probabilities $|R_{\uparrow\downarrow}(\lambda)|^2$ were also measured at $\delta\phi$=1.06mrd for two magnitudes of the external magnetic field (fig.5). The position and spectral width of the functions $R_{\uparrow\downarrow}(\lambda)$ corroborate the expected theoretical dependence $\Delta\phi\propto B\lambda^2$. It is evident that measurment of nondiagonal elements $|R_{\uparrow\downarrow}(\lambda)|^2$ in a wide spectral interval of λ and in the off-specular direction requires detector with wide angular aperture contrarily to the measurment of the sum $N_+R_{++}(\lambda) + N_-R_{-+}(\lambda))$ in the specular direction.

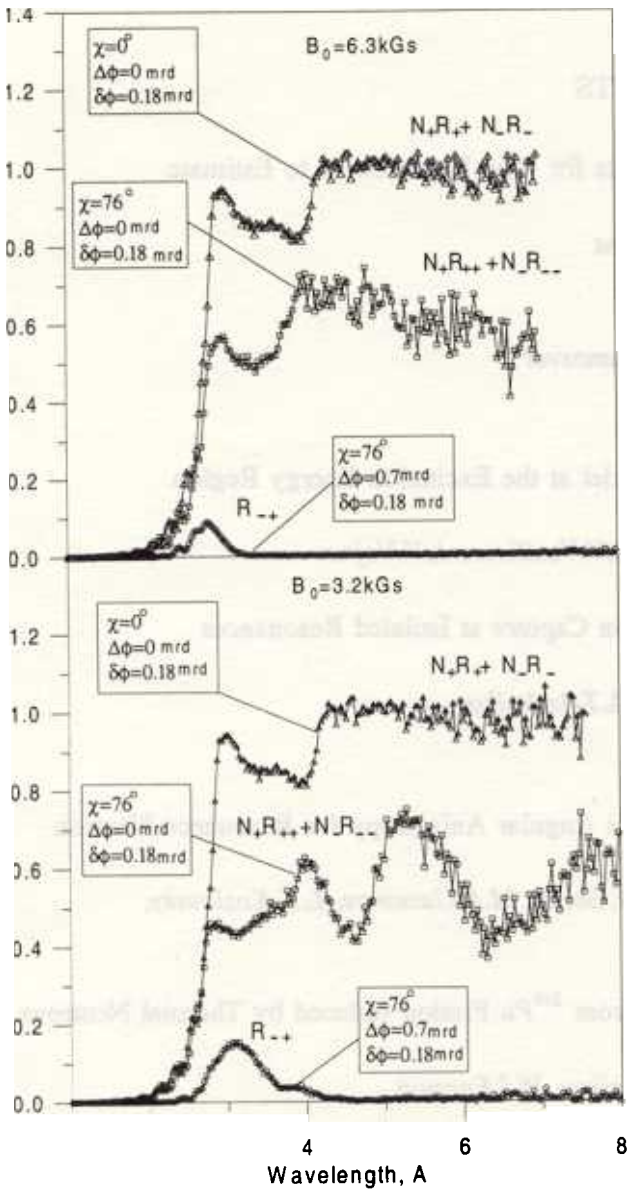

Fig.4. The wavelength dependence of $N_+R_{++}N_-R_-$ in the specular direction $\phi=\phi_0$ for $\chi=0$ and $\chi=76$deg. and of $|R_{-+}|^2$ for $\chi=76$deg in the off-specular direction ($\Delta\phi=0.7$mrd.). a) B=6.3kGs, b) B=3.2kGs.

§5. Conclusion

The obtained experimental data demonstrate that the relectometry in high external fields (B>2kGs) from noncollinear structures with nondiagonal reflection matrices reveals strong angular dispersion of the reflected neutrons with reversed spins. For the case of nonpolarized incident beam the observation of this dispersion gives the opportunity to measure the nondiagonal elements $R_{\phi(\omega)}(\lambda)$ in the off-specular beams and the sum $1/2(R_{++}(\lambda)+R_{--}(\lambda))$ in the specular one. It also gives the opportunity to get information on the distribution of magnetization in films using nonpolarized neutrons.

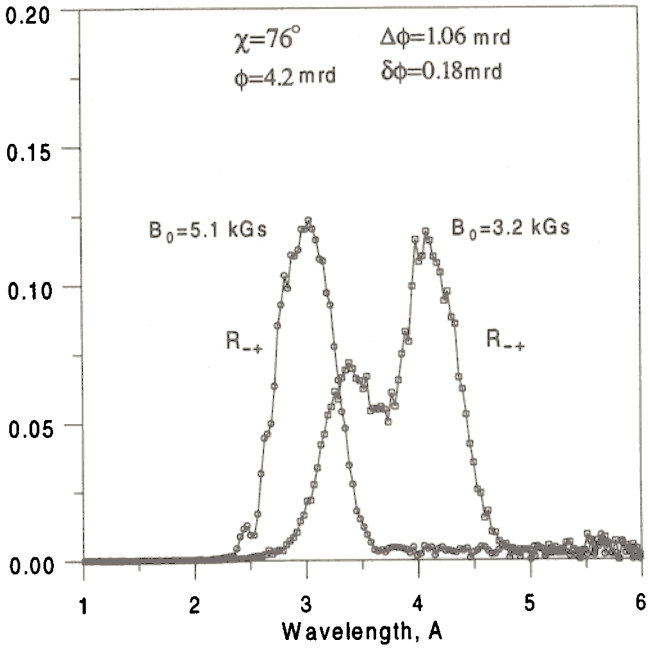

Fig.5 The dependence of $|R_{-+}|^2$ on λ for $\Delta\phi=1.06$mrd and two fields: B=5.1 kGs, and B=3.2kGs. The shift and broadeniag of the spectral interval for the weaker field corroborate the dependence $\Delta\phi\propto B\lambda^2$. The bell shaped forms of both spectra are related to the small aperture $\delta\phi=0.18$mrd of the detector.

Acknowledgments

One of the authors (V.K.I.) wants to express his gratitude to I.Carron for his invaluable assistance.

1) Hughes D.J., Burgy M.T., Phys. Rev. 81 (1951) 498.
2) Felcher G.P., Hildeke R.O., Crawford R. Haumann J., Kleb R. and Ostrowski G. Rev.Sci.Instr. **58** (1987) 609.
3) Korneev D.A., Pasyuk V.V., Petrenko A.V., and Dokukin E.B., "Neutron refectivity studies on superconducting, magnetic and absorbing thin films on the polarized neutron spectrometer at the pulsed reactor IBR-2" in H.Zabel,I.K.Robinson(Eds.) "Surface X-ray and neutron scattering" (Proceedings of the 2nd Int.Conf.,Bad Honnef, Germany, June 25-28, 1991), p.213-217
4) Lauter H.J., Bland J.A.C., Bateson R.D., and Jonson A.D. "Magnetic properties of ultrathin Co/Ag films investigated by polarized neutron reflection" Ibid, p. 219
5) Endoh Y., "Neutron reflection studies on magnetic superlattice", in Neutron Optics Devices and Applications, C.Majkrzak, J.Wood, Editors, Proc. SPIE 1738, 224-232 (1992)
6) Fitzimmons M.R., Smith G.S., Pynn R., Nastasi M.A., Burkel E. Physica B **198** (1994) 169.
7) Ignatovich V.K. Pis'ma ZhETP **28** (1978) 311 (see Sov. JETP Lett.).
8) Korneev D.A. Poverchnost' **2** (1989) 13 (in Russian).
9) Ignatovich V.K. "The Physics of Ultracold Neutrons" Claren-don Press, Oxford, 1990.
10) Majkrzak C.F. "Polarized neutron reflectometry" Physica B **173** (1991) 75.
11) Korneev D.A., Chernenko L.P. "Neutron diffraction opticsof films with noncollinear magnetic depth structure", in Neutron Optics Devices and Applications, C.Majkrzak, J.Wood, Editors, Proc. SPIE 1738, 468-476 (1992)
12) Zabel H. " Spin polarized neutron reflectometry of magnetic films and superlattices" Physica B 198 (1994) 156.